Nano Today xxx (xxxx) xxx

Contents lists available at ScienceDirect

Nano Today

journal homepage: www.elsevier.com/locate/nanotoday

Review

On-chip micro/nano devices for energy conversion and storage

Xuelei Pan[a,1], Xufeng Hong[a,1], Lin Xu[a], Yanxi Li[b], Mengyu Yan[c], Liqiang Mai[a,*]

[a] State Key Laboratory of Advanced Technology for Materials Synthesis and Processing, International School of Materials Science and Engineering, Wuhan University of Technology, Wuhan 430070, PR China
[b] Department of Material Science and Engineering, Stanford University, Stanford, California 94305, United States
[c] Materials Science and Engineering Department, University of Washington, Seattle, WA 98195-2120, United States

ARTICLE INFO

Article history:
Received 27 February 2019
Received in revised form 3 May 2019
Accepted 13 August 2019
Available online xxx

Keywords:
On-chip devices
In situ
Nanomaterials
Energy conversion
Energy storage

ABSTRACT

The evolution of next-generation energy technologies is growing in importance as the global demand for energy skyrockets. Nanotechnology and nanomaterials are critical in the creation of next-generation energy technologies. However, it is currently highly problematic to elucidate the unique properties of nanomaterials by conventional characterization methods. Hence, tailored micro/nano devices present potentially powerful opportunities as significant proof-of-principle tools for investigating the essential structures and properties of nanomaterials. Meanwhile, these devices became increasingly sophisticated in their ability to monitor individual nanomaterials under operando conditions. This review summarizes recent progress of on-chip micro/nano devices with a particular focus on their function in energy technology. Recent studies on energy conversion devices and electrochemical energy storage devices are introduced and the special design/role of these devices are emphasized. It is expected that this review will promote further research and broaden the applications potential of on-chip micro/nano devices, thus contributing to the development of energy conversion and storage technologies.

Contents

Introduction

As society advances in terms of both growing energy needs and reducing environmental footprint, the evolution of next-generation energy technologies is becoming increasingly significant [1,2]. And given the myriad of current and looming problems associated with climate change, the scientific and engineering communities are

* Corresponding author.
E-mail address: mlq518@whut.edu.cn (L. Mai).
[1] These authors contribute equally to this work.

https://doi.org/10.1016/j.nantod.2019.100764
1748-0132/

striving to develop cleaner/greener energy sources that could slow the progress of global warming—while at the same time ensuring energy security and a ready supply of power [3,4]. In terms of energy conversion, most of alternative sources of energy should eventually be converted to electricity that can be conveniently used and stored [5,6]. When considering energy conversion, efficiency remains a fundamental factor that must be taken into account, and researchers are pursuing such avenues in more eco-friendly ways [7]. In terms of energy storage [8], for instance, electrochemical devices such as batteries [9–13] and electrochemical capacitors [14–17] are widely used to store energy. In order to develop high-performance devices, one needs to consider certain factors—namely, the energy density, power density, rate performance, and cycling performance [11,18–20]. However, it remains challenging to successfully address these various demands while also accommodating the growing energy requirements of the public [21–24]. Commonly, it is attributed to the slow development of key functional materials that is disjointed to the rapid increasing energy demand [25].

In recent decades, the realm of nanotechnology has been playing an ever-increasing role in advancing the energy science and technologies [26–32]. Indeed, the application of nanomaterials represents somewhat of a milestone in the development of next-generation energy conversion and storage capabilities [33,34]. As a general definition, nanomaterials feature at least one dimension that is sized between 1 and 100 nm. Depending on their size, nanomaterials are endowed with geometrical advantages for measurement and characterization under operando conditions [35,36]. Meanwhile, in practical energy devices, functional material components are fabricated by specific processing methods in order to obtain enough tap density and mechanical properties. [37,38] Undoubtedly, the unique properties of nanomaterials will be suppressed by traditional processing methods to some extent [39,40]. Although extensive of advanced nanomaterials have been developed for energy conversion and storage, the evaluation methodology has always been following the traditional methods which fabricate materials in bulk and test by practical macro devices [41]. This evaluation methodology pays more attention to the application potential and the aggregate properties while neglects the uniqueness of nanomaterial itself (*e.g.*, reduced dimensions and confined electronic properties). In physics communities, researchers have been devoted to studying the novel physical phenomena by on-chip micro/nano devices as they can detect the signal from specific low dimensional material with controlled thickness, size, crystal orientation, heterostructure, external field, *etc* [42–47]. Nevertheless, on-chip micro/nano devices haven't been widely applied in the field of energy conversion and storage. This may be attributed to the complex configurations of energy devices and the immature theoretical model. For instance, a typical lithium ion battery consists of positive electrode, negative electrode, electrolyte, current collector and membrane [48,49]. How to simplify these complex practical configurations (with electrochemical reaction) to a simple model in a micro/nano device was the first problem, especially in a single nanowire electrode system [50]. The second problem lies in how to get precise and high-quality signal of the individual nanomaterial under such complex conditions. The third problem is what important information can be achieved by on-chip devices. It is well-known that the evolution of nanomaterials has given birth to new characterization and diagnosis approaches [51–56]. Researchers have successfully addressed these three problems by well-designed on-chip devices and combing them with advanced characterization/measurement technologies. Firstly, the basic configuration of common energy conversion and storage devices is functional material-based closed circuit, which can be realized through modified on-chip physical devices fabricated by conventional microelectronics technology. Secondly, due to the high internal impedance (megohm) and small current level (picoamps or nanoamps), amplifying circuit and valid encapsulation are applied to get precise signals from individual nanomaterials. Thirdly, the importance of on-chip micro/nano devices are incarnated in the ability to focus on the specific region and materials and get real-time signal to investigate the information of materials.

This review aims to summarize the progress of on-chip micro/nano devices for energy technologies and present the fundamental methodology for designing and fabricating on-chip devices for *in situ* characterization or practical application. Herein, we focus on micro/nano devices, especially individual nanomaterial devices, which can play a critical role in investigating and determining special physicochemical properties in depth. These devices provide a platform for fully developing the natural advantages of nanomaterials, including the ability to obtain highly accurate measurements and *in-situ* monitoring of the characteristics of electrode materials in electrical/electrochemical processes. [11,50] It is worth noting that when designing the on-chip micro/nano device, the microfabrication processes are mainly depended on the detailed problems and limited by the combined characterization methods. Hence, the scope of this review is to give a systematic summary of fundamental application and architectures of on-chip micro/nanodevices, which is expected to favor the further research in energy-based materials science and technologies.

In this review, we present recent progress on advances in nanomaterial-based micro/nano devices from two perspectives: energy conversion and energy storage. The typical design and application of micro/nano devices are emphasized. In the field of energy conversion, we review photovoltaic devices, photoelectrochemical devices, thermo-electric devices, electrodialysis and blue energy devices, and electrocatalytic devices. In the field of energy storage, research on single nanowire electrochemical devices, individual nanosheet electrochemical devices, and on-chip micro-supercapacitors are presented. Finally, a brief analysis of current on-chip devices is provided, followed by a discussion of the future development of micro/nano devices. It should be noted that, we have weakened the in-depth analysis of performance data, but focus on exploiting the relationship among the device structure, the unique material properties and characterization methods.

On-chip micro/nano energy devices

As a functional material for energy conversion and storage, it should be integrated into specific device with essential configuration and structure to realize basic functions. It is necessary to make it clear that different devices have different structures and functions. The comparison of practical devices, experimental devices and on-chip devices are shown in Fig. 1a-c. Three examples, solar cell, fuel cell and Li-ion battery are compared with the corresponding experimental devices and on-chip micro/nano devices with simplified configuration. For practical application, energy devices aim for daily using, and should satisfy the requirement industrial manufacture and customer. [57,58] For basic scientific research, energy devices can be thought as prototype devices with simplified components, which facilitates the precise measurement and principle validation [59,60]. Herein, on-chip micro/nano devices should be assigned to a kind of research-oriented devices but essentially different from conventional experimental devices [61]. In a typical on-chip micro/nano device, active material is the core. That means the essence of the complex on-chip device is to extract and record the signal of specific materials and local regions, especially individual nanomaterial. The energy-based on-chip micro/nano devices initially rooted in physical devices and gradually developed into unique and significant research platform.

Please cite this article in press as: X. Pan, et al., On-chip micro/nano devices for energy conversion and storage, Nano Today (xxxx), https://doi.org/10.1016/j.nantod.2019.100764

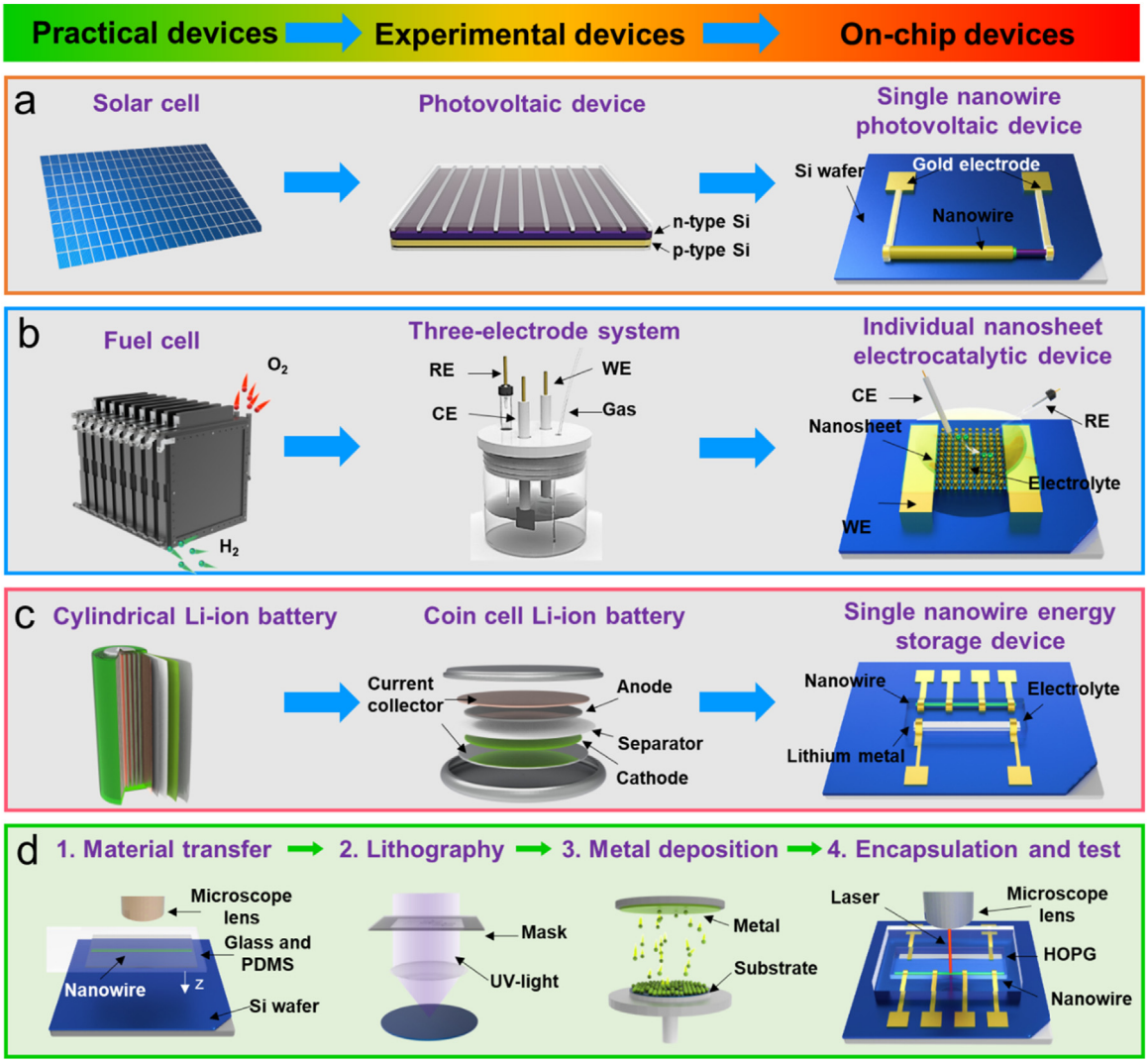

Fig. 1. The comparison of practical devices, experimental devices and on-chip devices. Three examples are presented: (a) Solar cell, photovoltaic device and single nanowire photovoltaic device; (b) Fuel cell, three-electrode system and individual nanosheet electrocatalytic device; (c) Cylindrical Li-ion battery, coin cell Li-ion battery and single nanowire energy storage device. The dominate components are labeled. The blue substrates represent silicon wafers. RE, CR, WE represent reference electrode, counter electrode and working electrode, respectively. (d) Four primary steps of fabricating the on-chip micro/nano devices by conventional microelectronic technologies. (This is an example of the fabrication process for single nanowire battery where the single nanowire and highly oriented pyrolytic graphite (HOPG) flakes work as cathode and anode, respectively. It is worth noting that these steps are not necessary for all devices.) The first step is materials transfer process by the pick-and-lift method, the second one is optical/e-beam lithography, the third one is metal deposition and the last one is encapsulation and test process. Through the presented four steps, a common on-chip micro/nano device can be fabricated and the basic measurement and characterization can be realized.

According to the recent literature, the general principles for designing and fabricating on-chip micro/nano devices are introduced (Fig. 1d). To obtain the direct signal of individual nanomaterial, a dielectric substrate is essential to serve as platform and micro-electrodes are applied to connect nanomaterials with measurement equipment. The fabrication process of an on-chip micro/nano device is similar as on-chip physical devices fabricated by micro-electronic technologies. The transfer process of material can be varied, such as spin coating [62], in-situ growth [63,64], pick-and-lift [65–67], where the essential difference among these transfer processes is the orientation deterministic. Micro-electrodes are commonly fabricated following a traditional optical/electron-beam lithography [60,68,69] and metal deposition method [70,71]. After linking nanomaterials in a circuitry, the basic unit for electrical measurement is completed. This is the basic configuration for a pure physical condition without chemical/electrochemical reactions. If the on-chip device has a three-dimensional architecture, the fabrication process will be more complex, the detailed examples will be presented in the following sections [63,64,72]. Specially, in an electrochemical system immersed liquid/ solid electrolyte, fabricating insulating layer (*e.g.*, PMMA, SU-8 and Si_3N_4) on metal electrodes is necessary to get pure signal from the selected material (micro reference and counter electrodes are usually needed). Although the aforementioned processes are basic condition in designing and fabricating on-chip micro/nano energy device, it is worth noting that these devices are objective-oriented and flexible. And when combined with *in-situ* characterization methods, some configuration should be adjusted to realize some special functions. In the next sections, the elaborate design for detecting special signals are summarized and the details are dissected.

Energy conversion devices

As a simple definition, energy conversion represents energy transferred between different locations or dissimilar objects with different forms. [73,74] The energy conversion process is comprised of two major phases: The first involves harvesting and convert-

Please cite this article in press as: X. Pan, et al., On-chip micro/nano devices for energy conversion and storage, Nano Today (xxxx), https://doi.org/10.1016/j.nantod.2019.100764

ing the primary energy source (solar, thermal, chemical, *etc.*) to a usable energy form (electricity or fuel), and the second involves energy consumption to power our homes, vehicles, devices, and so on. In terms of sustainability and abundance, solar energy surpasses all other sources as the most promising energy source. [75,76] Nonetheless, solar energy needs to be converted to electricity mainly through photovoltaic devices for large-scale and long-time use and storage. In a typical energy conversion process, a solar cell is used for energy harvesting, a battery for energy storage, and the cycle concludes with energy consumption in the form of electricity.

It bears repeating that when considering energy conversion, one of the most important issues is efficiency. This reality highlights the need to develop more efficient energy-conversion devices, which increasingly refers to small, compact devices that are sufficiently power for today's energy needs. To promote energy conversion efficiency, micro/nano materials have shown great potential. Macro-sized energy devices are suitable for confirming validity (*i.e.*, high efficiency and stability) of the specific materials and their practical configurations. However, when elucidating the basic principles and scientific laws of these conversions or reactions, they will be ineffective, especially for micro/nano-sized materials. Accordingly, micro/nano devices are playing an increasingly critical role and are expected to produce many exciting outcomes. In this section, a range of micro/nano devices with applicability for energy conversion processes, involving solar energy, thermal energy, chemical energy and blue energy, are presented.

Photovoltaic devices

As a green, renewable energy source, solar energy continues to attract wide attention for its vast potential. Although huge quantities of energy radiate to the Earth in the form of sunlight, however, the amount of energy currently collected and converted to energy represents a tiny fraction of overall energy consumption. Hence, it is very urgent to increase the efficiency of solar energy conversion. [77,78] Third-generation photovoltaic technologies target at low cost and higher efficiency, which points to enormous opportunities for the development of advanced nanowire-based solar cells. [79,80] Coaxial nanowires, made up of p-type, intrinsic and n-type (p-i-n) semiconductors, have been proven to increase the carrier collection and the efficiency of solar cells, which is attributed to the long axis light adsorption and short radial carrier separation [55,81]. Due to these advantages, nanowire photovoltaics continue to attract attention. Meanwhile, the complex motifs of nanowire heterostructures (axial, radial and p-n/p-i-n nanowires) become important problems for developing novel nanowire-based solar cells. As a prototypical research platform, single nanowire devices enable the measurement of intrinsic characteristics and performance of different structure motifs of a single nanowire with accurate quantitative research, which is why single nanowire photovoltaics have been studied in experiment and theory over the past decade [55,82].

As far back as 2007, the Lieber Group reported a single p-i-n silicon nanowire solar cell capable of driving an on-chip nanosystem [83]. To fabricate a single p-i-n silicon nanowire device, coaxial silicon nanowires are synthesized and etched selectively (Fig. 2a). This device enables characterization of photovoltaic properties for a single coaxial nanowire. Experimental results (Fig. 2b) demonstrate that a single p-i-n silicon nanowire can supply a short-circuit current of 0.503 nA and voltage of 0.206 V. The output power reaches ~72 pW at 1-sun illumination. Such a device can also drive a nanowire-based AND logic gate, which shows promise for self-powered nanosystems. In 2009, the Lieber Group described a single n-GaN/i-InxGa1-xN/p-GaN core/shell/shell nanowire photovoltaics device, which enabled them to painstakingly define the intrinsic limits of the III-nitride materials system. This device was the first coaxial III-nitride nanowire photovoltaic device with enhanced efficiencies, which can be attributed to a high-quality quantum well in the InGaN/GaN nanowire structure—an advance that cannot be achieved in planar devices because of the lattice mismatch.

In addition to the lying nanowire devices, standing nanowire devices also attract quite attention. A standing nanowire device represents a simplified model for nanowire array, while it also means complicated three-dimensional architecture in device. In 2013, Krogstrup et al. reported a single standing GaAs nanowire solar cell. [63] In this work, coaxial p-i-n GaAs nanowires positioned on a silicon wafer were fabricated *via* the epitaxial growth method (Fig. 2c). The inner core is p-type, which is Be-doped, and the outer shell is n-type, which is Si-doped. SU-8 photoresist was used as the filler and indium tin oxide (ITO) was used as the top electrode (Fig. 2d). The current-voltage characteristics of the device are shown in Fig. 2e. External quantum efficiency (EQE) results demonstrate that standing nanowires exhibit ~7-fold high efficiency when compared to lying nanowires (considering the highest value). Researchers also confirmed that the absorption area had increased over the apparent cross-section area of nanowires. It is thought that the GaAs nanowire exhibits resonance since the diameter is comparable to the radiation wavelength, which increases the total absorption of light. These factors contributed to the record-breaking maximum efficiency that surpassed the Shockley-Queisser limit.

Although the single nanowire solar cell achieved high conversion efficiency, a standard assessment criteria for the conversion efficiency of a single nanowire has yet to be proposed. [84] As is demonstrated above, the subwavelength nanowire will enhance light absorption, which makes calculating conversion efficiency difficult due to the differences between geometric dimensioning and real absorption scale. Thus, it is essential to make the single nanowire device comparable to the macroscopic-scale device. Mann et al. used InP nanowire as a model to elucidate both the intrinsic performance of a single nanowire solar cell [85] (Fig. 2f), as well as associated performance loss mechanisms. [86] Firstly, they solved the problem of metrics by using an integrating sphere microscopy set-up, which enables the standard absorbed power measurement (Fig. 2h). Then they measured the quantum efficiency and photoluminescence quantum yield of single nanowire using this set up. To normalize the EQE of this single nanowire solar cell, they defined the EQE according to the absorption width, since the effective absorption width is a function of incident wavelength and angle. Interestingly, they obtained a high open circuit voltage (up to 0.85 V, 73% of the thermodynamic limit) and a high efficiency of photocurrent collection (Fig. 2g). Additionally, this device is convenient for detecting the mechanisms associated with energy loss. The researchers attributed the open-circuit voltage loss to two factors: non-radiative recombination and contact resistance. It should also be noted that this work employed an integrated device consisting of a single nanowire device and sphere microscopy to achieve their quantitative measurements of the device's quantum efficiency, which represents a powerful tool for exploring the mechanisms that drive the successful use of nanowire-based photovoltaic devices.

Photoelectrochemical devices

In addition to solar-to-electricity conversion, solar-to-fuel conversion is also an important method for utilizing solar energy. [87–89] A growing body of research has been devoted to studying this process due to its heightened efficiency [90–92]. In particular, discovering the intrinsic properties of nanowires for use in a single-nanowire device will advance such studies. For example,

Please cite this article in press as: X. Pan, et al., On-chip micro/nano devices for energy conversion and storage, Nano Today (xxxx), https://doi.org/10.1016/j.nantod.2019.100764

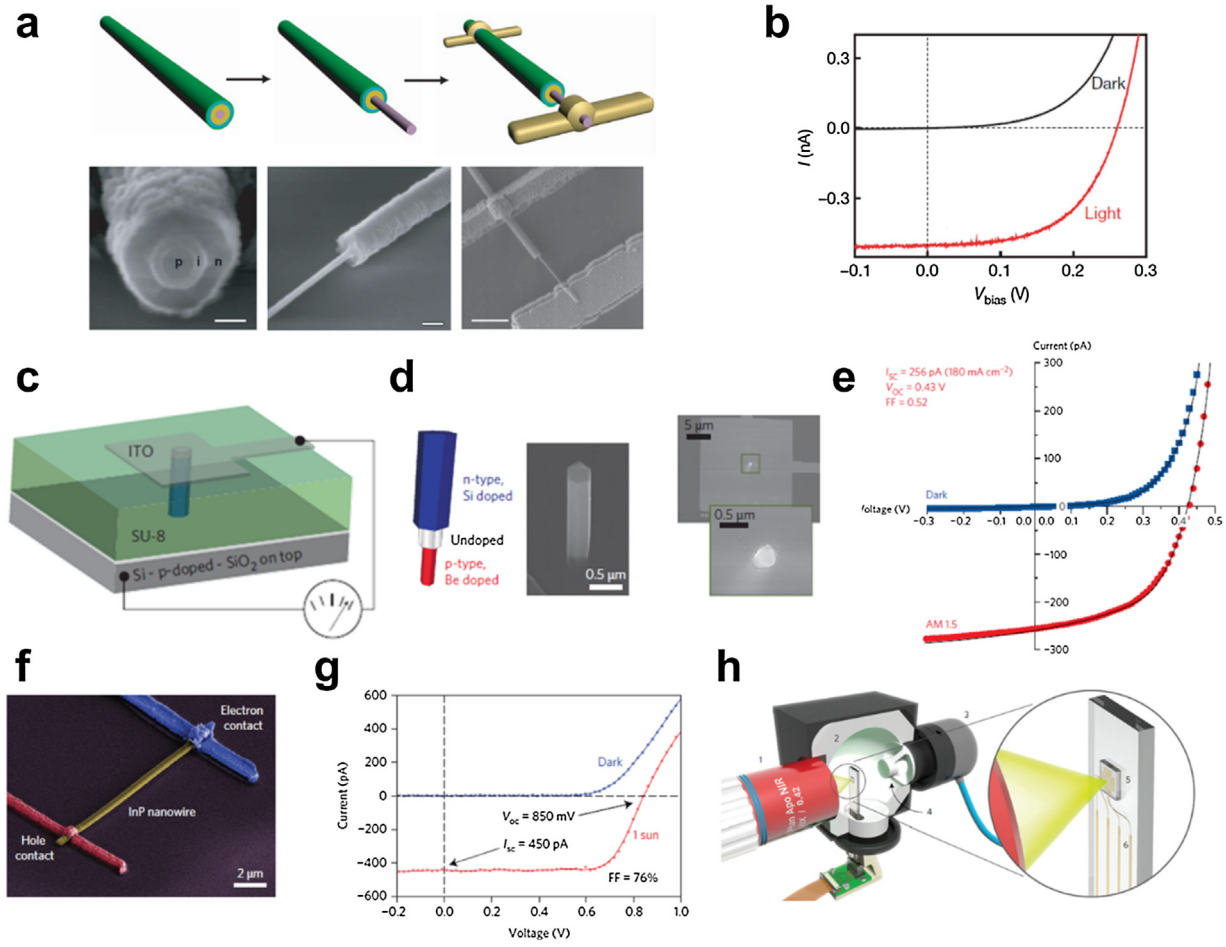

Fig. 2. (a) Schematics of fabrication process of the single nanowire photovoltaic device. Left, pink, yellow, cyan and green layers correspond to the p-core, i-shell, n-shell and PECVD-coated SiO_2, respectively. Middle, selective etching to expose the p-core. Right, metal contacts deposited on the p-core and n-shell. Bottom, SEM images corresponding to schematics in a. Scale bars are 100 nm (left), 200 nm (middle) and 1.5 μm (right). (b) Dark and light *I–V* curves of p-i-n Si nanowire. Reproduced with permission. [83] Copyright 2007, Nature Publishing Group. (c) Schematic of the vertical single-nanowire radial p-i-n device connected to a p-type doped silicon wafer by epitaxial growth. (d) Left: doping structure of the nanowire. The p-type doped core is in contact with the doped silicon substrate and the n-type doped shell is in contact with the ITO. Right: Scanning electron microscope (SEM) image of a nanowire solar cell before adding the top contact. The nanowire is ~2.5 μm high and has a diameter of ~425 nm. (e) Current-voltage characteristics of the device in the dark and under AM 1.5 G illumination, showing the figure-of-merit characteristics. Reproduced with permission [63]. Copyright 2013, Nature Publishing Group. (f) False-color SEM image of the InP nanowire device (yellow) with the hole contact (red) and electron contact (blue). (g) The nanowire *I–V* curve in the dark (blue) and under the solar simulator at 1 sun intensity (red). The solid line is a smoothed fit to the data points (shown as small crosses). (h) A schematic depicting the integrating sphere microscopy set-up. Reproduced with permission. [86] Copyright 2016, Nature Publishing Group.

the Yang Group designed a single vertically aligned nanowire photoelectrochemical device (as shown in Fig. 3a). [64] The silicon nanowires, which were vertically positioned on a silicon-on-insulator (SOI) substrate, were fabricated by the vapor-liquid-solid growth method and then underwent p-type and n-type doping (Fig. 3b). The researchers loaded platinum on silicon nanowires by electro-deposition to form a typical photoelectrochemical system, in which platinum and silicon serve as the electrocatalyst and light absorbing electrode, respectively. The schematic of device is presented in Fig. 3c. This system also employed SU-8 as the insulating layer in order to ensure accurate measurement in aqueous electrolyte. They then measured different individual nanowires, which show broad distribution of photovoltage (Fig. 3d). However, when these nanowires were connected in parallel, the output photovoltage displayed an obvious "short-board effect", *i.e.*, the typical output voltage will be decided by the nanowire with lowest photovoltage. Subsequently, they investigated the determining factor for the significant variance. Owing to the single-nanowire-based measurement, the quantitative analysis shows that the photo-generated electron flux represents a function of length and diameter. These results demonstrated that a single nanowire device can serve as a well-defined model system for advancing the field of photoelectrochemistry.

In addition to nanowire materials, 2D crystals also play a special role in the field of photoelectrochemistry—principally due to their abundant surface-active sites and rapid electron transport in plane, [93,94] which shows promise for energy conversion, sensors, and catalysts. Although the photoelectrochemical behavior of 2D materials is fascinating, traditional methods lack the sophistication to precisely measure the photoelectrochemical properties of 2D materials due to the ensemble averaging results caused by testing more than one isolated piece of 2D material. Hence, measuring an isolated nanosheet or an individual nanosheet represents a far more effective approach. Generally, a standard photoelectrochemistry measurement system needs a light source and three-electrode system. Herein, an individual nanosheet works as a working electrode, whose size may range from ~1 μm to ~100 μm. For nanosheets sized less than 50 μm, it is better to measure the whole nanosheet. The traditional configuration is to utilize a micro-reference electrode and a counter electrode to measure the electrochemical properties of the immersed individual nanosheet. In contrast, for a nanosheet that is approximately 100 μm or larger, there is an alternative con-

Please cite this article in press as: X. Pan, et al., On-chip micro/nano devices for energy conversion and storage, Nano Today (xxxx), https://doi.org/10.1016/j.nantod.2019.100764

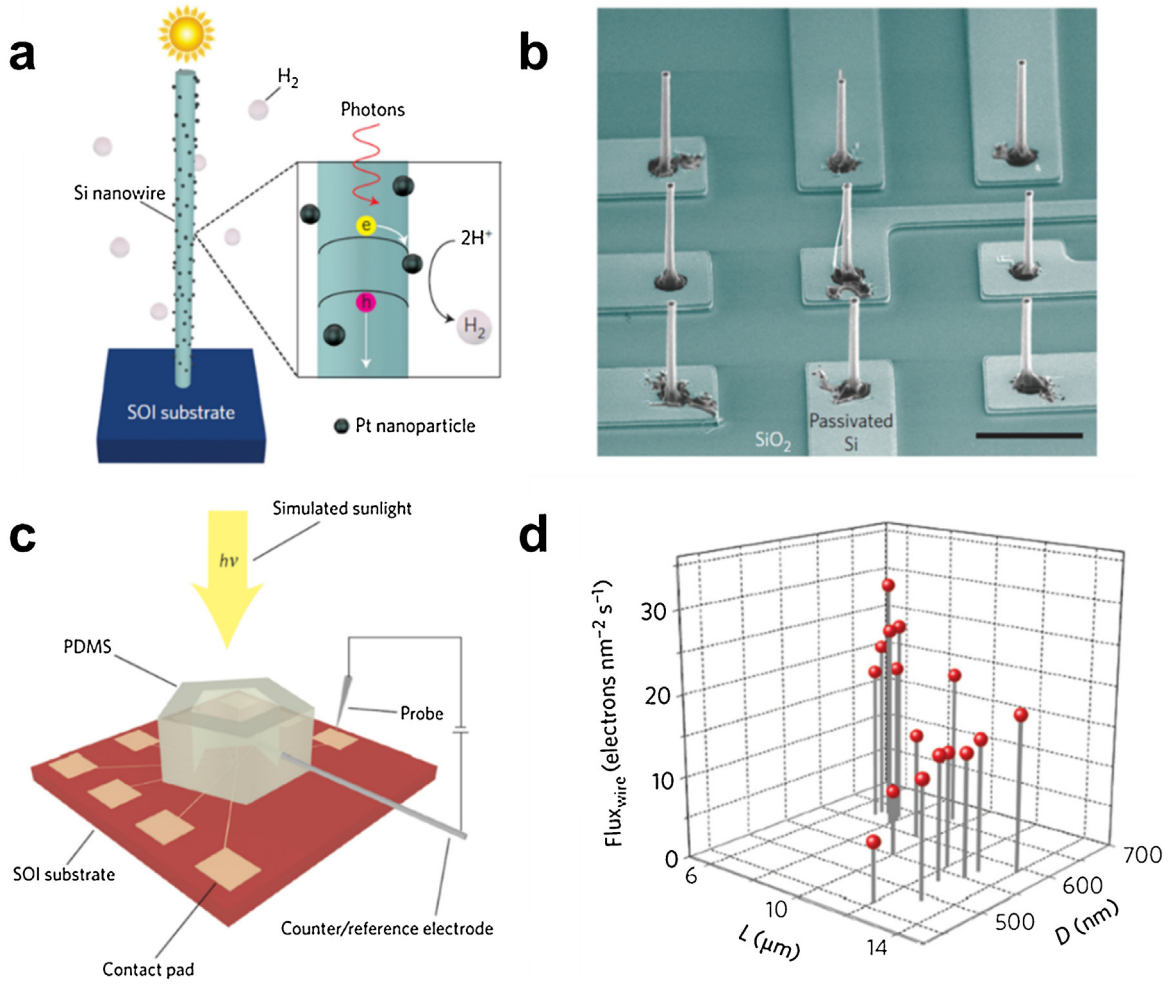

Fig. 3. (a) Schematic of the single silicon nanowire for the PEC process. Under illumination, photoexcited electron-hole pairs are produced and subsequently separated at the nanowire/electrolyte interface because of band bending. The electrons then move to the platinum catalytic sites and carry out proton reduction. (b) SEM image of individually addressable single nanowires. The silicon layer of the SOI substrate is patterned into nine electrically isolated, oxide-passivated electrodes, with an oxide layer underneath. The single silicon nanowires are vertically grown on these isolated silicon electrodes by the VLS mechanism. Scale bar, 10 μm. (c) The PEC measurement scheme. A two-electrode configuration is used to characterize the *I–V* properties of single nanowires. The silicon nanowire serves as the working electrode, and a platinum wire functions as the counter/reference electrode. The reactor volume in which the PEC processes occur is defined by a polydimethylsiloxane (PDMS) chamber. A probe makes electrical contact with each nanowire through the outside pads, and the chamber is illuminated from above. (d) Statistical distribution of saturated $Flux_{wire}$ as a function of L and D of individual nanowires. Each data point represents a repeatable measurement of one single-nanowire device. Reproduced with permission. [64] Copyright 2016, Nature Publishing Group.

figuration. Based on a big plane area, a micropipette combined with micro-injector can be used to inject a micro-droplet with a diameter of ~20 μm, which is then able to obtain a partial measurement. It must be noted, however, that the micro-droplet will undergo severe evaporation if the concentration is not high enough due to its colligative properties. Thus, a highly-concentrated electrolyte and an ultrafine capillary tube-based electrode are required for achieving accurate measurements. Based on their similar operating principles, such a device can be considered to be comparable to a scanning electrochemical microscope. In most cases, these two configurations can be used to measure electrochemical behavior of individual nanosheet and they are easily combined with a solar simulator.

The Geim Group used the second configuration to study the electrochemical properties of some typical 2D materials, *e.g.*, graphene [95–98] and MoS_2 [99,100]. In 2016, they reported a MoS_2 nanosheet-based photoelectrochemical device. [100] Specifically, they exfoliated large MoS_2 flakes with large lateral dimensions and a broad range of height dimensions on one plane, from monolayer to bulk (> 50 layers). This configuration enables *in situ* localized measurement of the electrochemical properties of MoS_2 with different layers under different irradiance (Fig. 4a). They used an outer-sphere mediator ($[Ru(NH_3)_6]^{3+/2+}$) to study the electron kinetics (ET) and used LiCl for the electric double-layer capacitance (EDLC) of MoS_2. Based on ET theory, the ET rate constant (k^0) can be calculated by the peak-to-peak separation. It is interesting that k^0 of bulk MoS_2 (1.95×10^{-3} cm s^{-1}) is much higher than the monolayer (~10^{-8} cm s^{-1}). In terms of bulk MoS_2, the k^0 displayed a linear relationship with the irradiance, but a nonlinear relationship for the monolayer MoS_2 (Fig. 4b). Also, the researchers confirmed a linear relationship between EDLC and irradiance for different samples. Although this method can obtain precise measurement, the actual test system is not ideal as there exists many defects, adsorbed groups and charge transfer resistance. Thus, further studies are needed to determine the potential of this system in obtaining accurate quantitative measurements.

Thermoelectric devices

The use of fossil fuels continues to account for a significant proportion of the world's energy generation and consumption, particularly in the developing world. [101] Unfortunately, the actual

Please cite this article in press as: X. Pan, et al., On-chip micro/nano devices for energy conversion and storage, Nano Today (xxxx), https://doi.org/10.1016/j.nantod.2019.100764

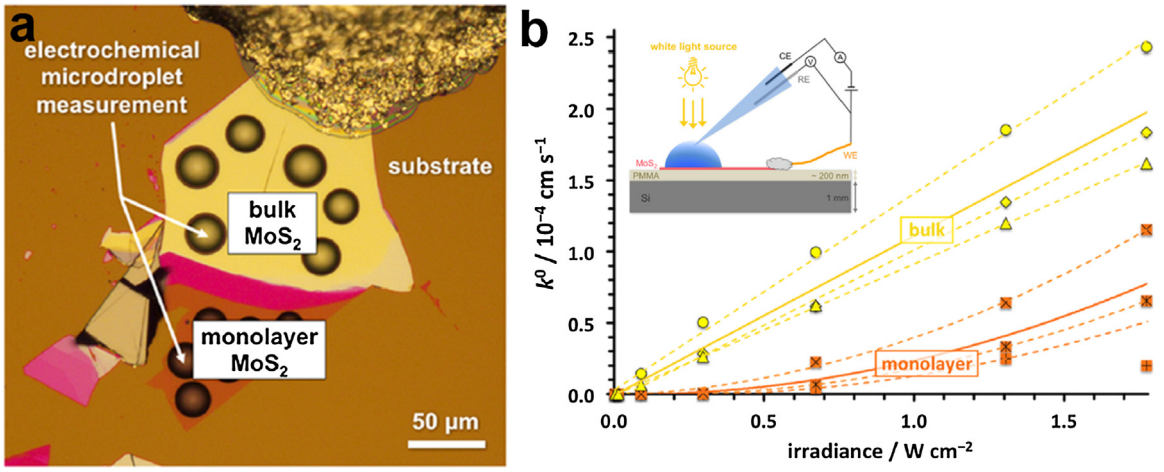

Fig. 4. (a) Optical micrograph of an MoS_2 flake on PMMA-coated Si substrate. (b) Dependence of the monolayer and bulk MoS_2 ET kinetics (k^0) on irradiance, determined from individual droplet measurements. Orange and yellow correspond to monolayer and bulk MoS_2, respectively, the dashed lines/curves are the best fits for the individual droplet measurements, and the solid lines represent the averaged response. The inset is the schematic of the photoelectrochemical setup. Reproduced with permission. [100] Copyright 2016, American Chemical Society.

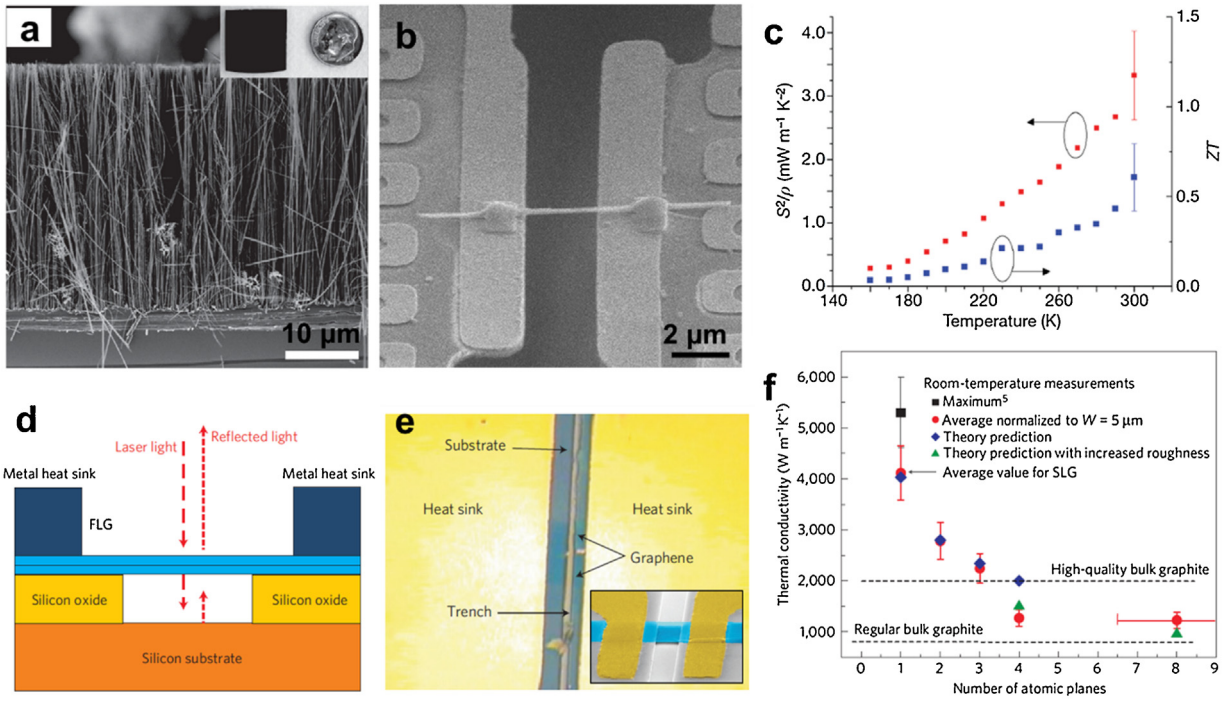

Fig. 5. (a) Cross-sectional SEM of an EE Si nanowire array, (b) An SEM image of a Pt-bonded EE Si nanowire (taken at 52 u tilt angle). The Pt thin film loops near both ends of the bridging wire are part of the resistive heating and sensing coils on opposite suspended membranes. Scale bar, 2 mm. (c) Single nanowire power factor (red squares) of the nanowire and calculated *ZT* (blue squares) using the measured k of the 52 nm nanowire. Reproduced with permission. [106] Copyright 2008, Nature Publishing Group. (d) Schematic of the thermal conductivity measurement showing suspended few-layer graphene (FLG) flakes and excitation laser light. (e) Optical microscopy images of FLG attached to metal heat sinks. Inset: colored scanning electron microscopy image of the suspended graphene flake to clarify a typical structure geometry. (f) Measured thermal conductivity as a function of the number of atomic planes in FLG. Reproduced with permission. [117] Copyright 2010, Nature Publishing Group.

efficiency of thermal power is merely 30%, since a large amount heat cannot be effectively utilized and therefore is lost [102]. Thermoelectric devices utilize the Seebeck effect of thermoelectric materials to convert thermal energy directly to electric energy [103]. Thermoelectric devices can use redundant heat and convert it to useful energy. A dimensionless figure of merit, *ZT*, is usually used to measure the performance of a thermoelectric material. The *ZT* value ($ZT = S^2\sigma T/k$) is determined by the Seebeck coefficient α, the conductivity c, and the thermal conductivity λ. The *ZT* value for a typical material barely reaches 1, whereas nanostructured materials can reach or exceed 1. [104] The merit and importance of nanowire thermoelectrics and the integrated devices have been comprehensively summarized by Chen et al in their recent review [105]. Herein, we present some typical work on nanowire (1D) and nanosheet (2D) thermoelectric devices. In 2008, Hochbaum et al. reported a Si nanowire thermoelectric device with a diameter of 50 nm whose thermal conductivity was reduced to 1/100 of that of bulk Si and the *ZT* value reached 0.6 at room temperature. [106] In this work, a wafer-scale Si nanowire array was prepared in $AgNO_3$ and HF aqueous solutions using an aqueous electroless etching [107] (EE) method. To test the thermal conductivity of a single nanowire, Hochbaum et al. assembled a single Si nanowire ther-

moelectric device (Fig. 5a). [106] First, a 200 nm SiN_x thin film was deposited on a silicon substrate, then the Si nanowire was fixed with Pt electrodes (Fig. 5b). The experimental results show that by optimizing the doping amount, nanowire diameter, and surface roughness, thermal conductivity is reduced, and the *ZT* value was significantly improved (the *ZT* data is shown in Fig. 5c). Due to the fact that the diameter of Si nanowires is less than the phonon mean free path, but more than the electron/hole mean free path, interface scattering of phonons is more intense than the electrons; hence, the *ZT* value has been increased.

Given the rapid development of nanomaterials, the need to accurately assess their basic physical properties (*e.g.*, thermal conduction [108]) has attracted a great deal of attention. [109] For layered materials, the layer-dependent variations in physical properties are very interesting [110–112]. Numerous theoretical and experimental results show that low-dimensional materials such as carbon nanotubes [113], carbon nanofiber [114], Si nanowire [115], and graphene [116], are completely different from bulk materials in terms of thermal conductivity. Individual nanosheet devices play a very important role in studying the thermal conductivity of low-dimensional materials. In 2010, Ghosh et al. systematically studied the thermal conductivity of graphene with different layers (Fig. 5d,e). [117] When the graphene layers increased from two to eight, the researchers observed a significant shift in thermal conductivity properties. As shown in Fig. 5f, when layer thickness increased from 2 layers to 4 layers, the thermal conductivity dramatically decreased from 2800 to 1300 $W m^{-1} K^{-1}$. This shift is attributed to the fact that when the number of graphene layers is few (2 – 3 layers), thermal conduction is mainly contributed by the non-harmonic vibration of the crystal lattice. In contrast, when the number of layers increases, the phonon scattering at the upper and lower boundaries between the layers leads to a decrease in thermal conductivity and, consequently, approaches the value of the bulk graphite. These experimental results obtained from monolithic graphene devices are of great significance for studying the thermal properties of low-dimensional materials.

Besides the fundamental measurement, on-chip devices also offer convenience for tuning electronic structures by introducing physical-field to tune more degrees of freedom. According to Hicks – Dresselhaus's theory [118,119], two-dimensional quantum confinement effect can greatly improve the power factors by enhancing electronic density of states. However, experimental verification was still a challenge for normal bulk materials. To give an experimental demonstration, Zeng et al. investigated the thermoelectric transport of 2D indium selenide (InSe) with different thickness and gate voltages [120]. In this devices, a microfabricated heater was used to supply temperature gradient, source and drain electrodes worked as thermometers and voltage probes. The optimal Seebeck coefficient and power factor of InSe nanosheet reach 570 $\mu V K^{-1}$ and 2.3 $mW m^{-1} K^{-2}$, respectively, when the thickness is 7 nm at 300 K. By identifying the thickness of InSe, the correlation between power factors and L/ξ is revealed (L, quantum confinement length; ξ, thermal de Broglie wavelength). This work gives valid experimental results to prove the role of quantum confinement and presents a practicable method for increasing the thermoelectric performance. Based on the on-chip devices, the unique properties of two-dimensional thermoelectric materials were thoroughly investigated, which shows great potential in the tunable electronic structures and confined sizes different from bulk materials.

Electrodialysis and blue energy devices

The Earth's oceans account for more than 70% of the planet's surface area. As such, seawater represents a potential rich source of energy. Moreover, seawater accounts for approximately 97% of global water reserves, leaving a very small percentage as freshwater reserves for an exploding global population competing for their living-giving resource. This urgent problem heightens the importance of developing viable seawater desalination processes. Electrodialysis (ED) desalination represents one of the efficient membrane-based methods for purifying seawater. [121] Specifically, ED is an electrochemical process in which an electrical field drive the ions separated through the membrane. In this way, a highly selective membrane is important for this approach [122]. As an important reverse process of ED, the osmotic pressure induced by the concentrate gradient between seawater and fresh water is able to produce energy. So-called "blue energy" utilizes seawater to produce electricity, which is a field that is gaining importance among researchers [123,124]. The fundamental theory of blue energy is the salinity gradients, which result in osmotic potential. [123] To convert salinity gradients directly, the ion exchange membrane is the key point.

2D materials offer good prospects for use in semipermeable membranes as their atomic thickness will reduce the most water transport. [125,126] Feng et al. reported a single-layer MoS_2-based blue energy generator (Fig. 6a). [127] Specifically, they used a free-standing single-layer MoS_2 with a single nanopore to fabricate the nanogenerator. This single-pore device reached dramatically high power density (10^6 $W m^{-2}$) with a KCl salt gradient, which is essentially impossible with a traditional membrane (Fig. 6b). In addition, they integraded this nanogenerator with a single-layer MoS_2 based transistor: one generator powered the drain and the other powered the gate (Fig. 6c). This self-powered system showed great performance as both a powerful generator and an efficient single-layer MoS_2 transistor. [47]

In addition to the use of MoS_2, graphene is also a great candidate for incorporation in an atomic-thick membrane. [128] Given its high ion-selectivity, porous graphene has been widely applied to the field of the electrodialysis desalination [129]. Indeed, a substantial body of work has been devoted to demonstrating the ion selectivity of porous graphene [130], such as K^+/Cl^- selectivity. [130] The common configuration for these studies (and especially those targeting single nanopore membranes) is an on-chip device based on an individual freestanding graphene with nanopores created by electron/ion bombardment and oxidation. Meanwhile, this on-chip device can be etched through the silicon wafer to obtain a micrometer-size hole, which enables the "real-freestanding" graphene (Fig. 6d). This hole-drill process involves wet chemical etching and reactive ion etching (RIE), which is intended to remove the large-scale Si layer, and the thin SiN_x, respectively. Thanks to the reliable Si wafer and the impermeable watertight treatment, this approach achieved a single nanopore membrane, as well as facilitated accurate measurements.

It has been demonstrated that a "perfect" graphene will not enable any atoms or molecules to permeate through it under ambient conditions due to the presence of a dense electronic cloud. [131] However, some researchers have confirmed that accelerated protons can transport through a single layer graphene. [132] The Geim Group investigated a series of monolayer crystals to explore the transport properties of protons through the atomic-thick layer [132]. They found that protons are able to transport through monolayer graphene and h-BN, demonstrating high proton conductivity. But for the monolayer MoS_2 and few-layer graphene and h-BN, thermal protons are not permeable (Fig. 6e,f). This phenomenon is attributed to the different electronic cloud, as well as the atomic configuration. Research shows that h-BN presents the best proton conductivity because of its strong polarization-induced local concentrated electrons around N atoms, which created a more porous electron cloud compared to monolayer graphene. The facilitated transport process of protons has significant application potential for fuel cell since it demands high proton conductivity to function.

Please cite this article in press as: X. Pan, et al., On-chip micro/nano devices for energy conversion and storage, Nano Today (xxxx), https://doi.org/10.1016/j.nantod.2019.100764

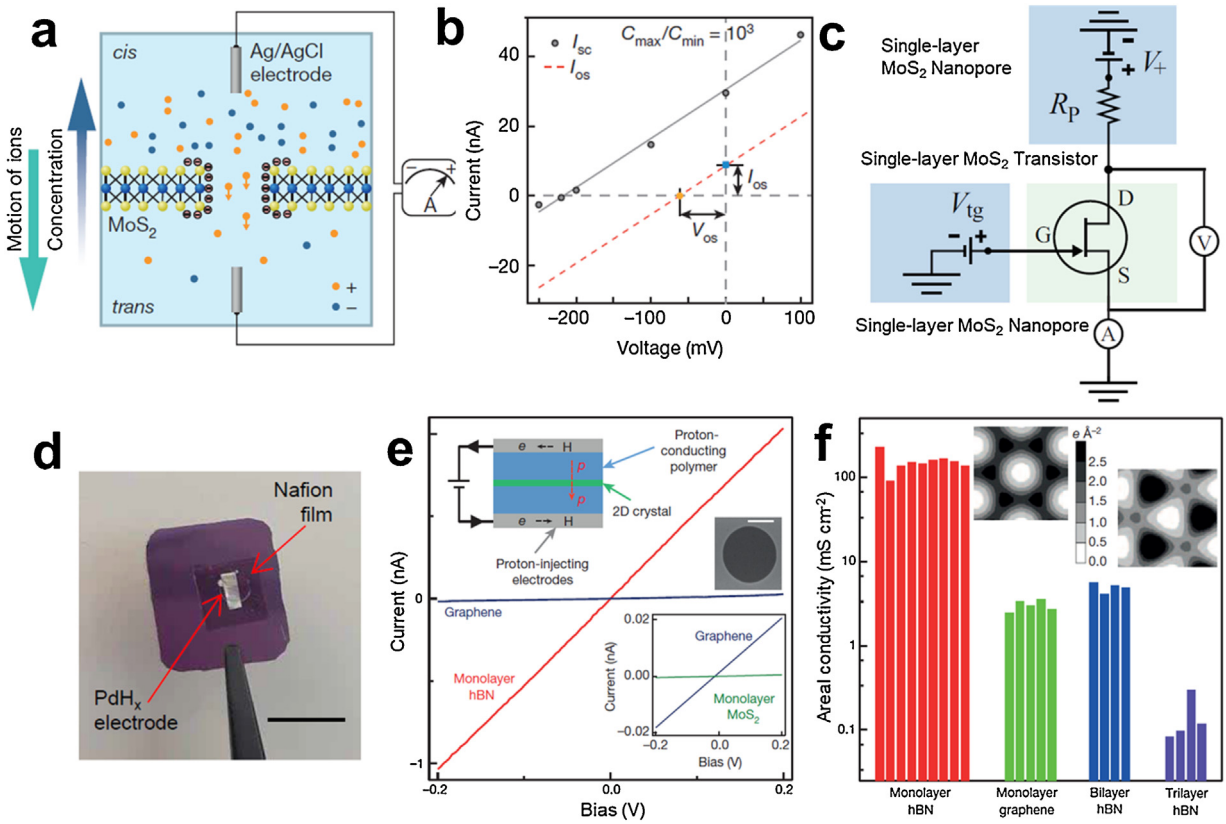

Fig. 6. (a) The experimental set-up. Salt solutions with different concentrations are separated by a 0.65-nm-thick MoS_2 nanopore membrane. An ion flux driven by chemical potential through the pore is screened by the negatively charged pore, forming a diffusion current composed of mostly positively charged ions. (b) Current-voltage characteristics for a 15-nm nanopore in a 1 M/1 mM KCl gradient. I_{sc} and V_{oc} are the short-circuit current and open-circuit voltage, respectively; I_{os} and V_{os} are the osmotic current and potential. (c) Electrical measurements with two nanopores (V_+, nanopore output voltage; V_{ds}, drain-source voltage; V_{tg}, top gate voltage). The voltage drop across the transistor channel is monitored with the voltmeter (V); current is measured with current amplifier (A). Reproduced with permission. [127] Copyright 2016, Nature Publishing Group. (d) Optical photo of the Silicon wafer based device. (e) Examples of *I–V* characteristics for monolayers of hBN, graphite and MoS_2. The upper inset shows a sketch of the experimental set-up. The middle inset (scale bar, 1 mm) shows an electron micrograph of a typical graphene membrane before the deposition of Nafion. Small (pA) currents observed for MoS_2 membrane devices (lower inset) are due to parasitic parallel conductance. (f) Histograms for 2D crystals that are found to exhibit measurable proton conductivity. Each bar represents a different sample with a 2 mm-diameter membrane. Insets: charge density (in electrons per $Å^2$) integrated along the direction perpendicular to graphene (left) and monolayer hBN (right). The white areas are minima at the hexagon centres; the maxima correspond to positions of C, B and N atoms. Reproduced with permission. [132] Copyright 2014, Nature Publishing Group.

Electrocatalytic devices

Hydrogen, which is described as the cleanest source of energy in the 21st century, has broad prospects due to its inherent natural advantages (*e.g.*, abundance, renewability, and high energy density). [133–135] Currently, the most efficient and feasible hydrogen production method involves electrolysis water splitting [136,137]. Electrolysis water splitting involves two half-reactions: hydrogen evolution reaction (HER) [133,138] and oxygen evolution reaction (OER) [139,140]. Precious metals (*e.g.*, platinum and palladium) show excellent electrocatalysis performance due to their negligible overpotential and fast reaction kinetics [134,141]. However, their escalating cost and scarce reverses severely limit their large-scale application [141,142]. The search for alternative high-performance electrocatalysts has become an important issue that has been widely studied [143]. Numerous studies have shown that molybdenum disulfide (MoS_2) is a promising electrocatalyst, which has moderate Gibbs free energy of H absorption (ΔG_H). [144,145] It is widely acknowledged that the edge sites of MoS_2 are the dominated active sites. [146,147] The first experimental demonstration used an indirect method that identified a linear relationship between the number of edge sites and HER activities of MoS_2 [146]. Nonetheless, the search for direct evidence of the actual active sites continues to be problematic. If one uses an individual MoS_2 nanosheet-based device, this issue can be easily demonstrated. For instance, Zhang et al. employed poly(methyl methacrylate) (PMMA) as a cover layer to form different exposure configurations (edge exposure or basal plan exposure) (Fig. 7a,b), which enables direct comparison and the precise measurement of reaction kinetics. [147] In a typical electrochemical system, electrocatalysis measurement is usually recorded by three-electrode configuration. In the on-chip device, one individual nanosheet (*e.g.* MoS_2 nanosheet) works as working electrode. Researchers have done extensive works on the design of this working electrode, such as contact resistance reduction, multi-electrode measurement, lateral/van der Waals heterostructure and local exposed construction. The details of these work are summarized and compared in Table 1.

Herein, we present some typical work which represent the recent progress of this flourishing field. Previous studies have shown that reducing the contact resistance between the electrode and the material can effectively enhance the charge injection to the catalyst and increase catalytic activity. [148–150] Voiry et al. designed electrochemical devices based on monolayer MoS_2 nanosheet to test the catalytic performance of MoS_2 with various contact resistances. [151] Using this device, treating the specific area with n-butyllithium is able to convert the MoS_2 from the semiconductive 2H phase to the metallic 1 T phase, thereby reducing contact resistance (Fig. 7c,d). Experimental results show that when contact resistance is negligible, the 2H phase MoS_2 with the edge covered and the 2H phase MoS_2 with the exposed edge both present

Please cite this article in press as: X. Pan, et al., On-chip micro/nano devices for energy conversion and storage, Nano Today (xxxx), https://doi.org/10.1016/j.nantod.2019.100764

Table 1
Summary of on-chip electrocatalytic devices.

Electrocatalysis	Materials	Preparation methods	Device configuration	Measurement design	Highlight	Ref.
HER	MoS_2 nanosheet	Chemical vapor deposition (CVD)	Individual nanosheet acts as working electrode, PMMA acts as insulating layer	Single-layer MoS_2 with edge covered and exposed, and 1 T-2H lateral heterostructure	Uncover the role of contact resistance and charge transport	[151]
HER	MoS_2 nanosheet	CVD	PMMA acts as insulating layer, 300 nm SiO_2 acts as dielectric layer	Gate dependent HER measurement	Surface electron concentration enhances HER performance	[159]
HER	MoS_2 nanosheet	Mechanical exfoliation	PMMA acts as insulating layer, 300 nm SiO_2 acts as dielectric layer	Individual MoS_2 sheet field effect transistor in electrochemical system	Enhance charge injection greatly improve HER performance	[160]
HER	MoS_2 nanosheet	CVD	PMMA acts as insulating layer	Local measurement of basal plane and edge of 2H and 1 T' phase MoS_2	Prove the Mo-terminated edge of 2H and 1 T' MoS_2 are active sites	[147]
HER	MoS_2 nanosheet	CVD	PMMA acts as insulating layer	Graphene and MoS_2 heterostructure with different contact forms	Demonstrate the role of electron transport with the catalyst	[164]
HER	MoS_2 nanosheet	CVD	PMMA acts as insulating layer	2H-2H and 2H-1 T domain boundary in basal plane	Domain boundaries in MoS_2 show remarkable HER performance	[202]
HER	MoS_2 nanosheet	Mechanical exfoliation	PMMA acts as insulating layer	Use Laser and annealing to realize different patterned devices	Prove crystal-phase-dependent electrocatalysis	[152]
HER	MoS_2 nanosheet	Mechanical exfoliation	PMMA acts as insulating layer	Introducing electric field and sunlight illumination	Enhance electron injection to the active sites contribute to faster charge transfer kinetics	[162]
HER	MoS_2 nanosheet	Mechanical exfoliation	PMMA acts as insulating layer	Eight-terminal device for the angle-resolved HER measurement	Report the in-plane anisotropic electrochemical properties of 1 T′-MoS_2	[203]
HER	VSe_2 nanosheet	Mechanical exfoliation	PMMA acts as insulating layer	Gate tuning the ions adsorption	Facilitate adsorption dynamics of HER	[161]
HER	WTe_2 nanosheet	Mechanical exfoliation	PMMA acts as insulating layer	Graphene and WTe_2 heterostructure exposing basal plane and (010) and (100) edge	Anisotropic electrical conductivity affects the HER performance	[163]
HER	$PtSe_2$ nanosheet	CVD	PMMA acts as insulating layer	$PtSe_2$ with different layer number and exposed states	Investigating the layer dependent HER performance	[204]
HER	MoS_2/WTe_2 heterostructure	CVD/ Mechanical exfoliation	PMMA acts as insulating layer	Different exposed states of MoS_2/WTe_2 heterostructure	Charge injection in through heterojunctions enhances HER performance	[205]
OER	Ni-graphene nanosheet	Hydrothermal method	SU-8 photoresist acts as insulating layer	Five-electrode device configuration (three working electrodes and one reference electrode and counter electrode)	Design the circuit of electrical transport spectroscopy to monitor the interface (*in situ* I–V measurement and on-chip electrochemical impedance spectroscopy measurement)	[62]
ORR	Pt nanowire	Hydrothermal method	PMMA acts as insulating layer	Four-electrode device configuration (source and drain electrode in electrochemical system)	In situ measurement of anionic surface adsorptions (sulfates, halides, and cyanides) on platinum nanowires.	[206]
Multiple electrochemical reactions	Pt nanowire	Hydrothermal method	PMMA acts as insulating layer	Four-electrode device configuration as above	On-chip electrical transport spectroscopy reveals the electrochemical interface information	[164]

Please cite this article in press as: X. Pan, et al., On-chip micro/nano devices for energy conversion and storage, Nano Today (xxxx), https://doi.org/10.1016/j.nantod.2019.100764

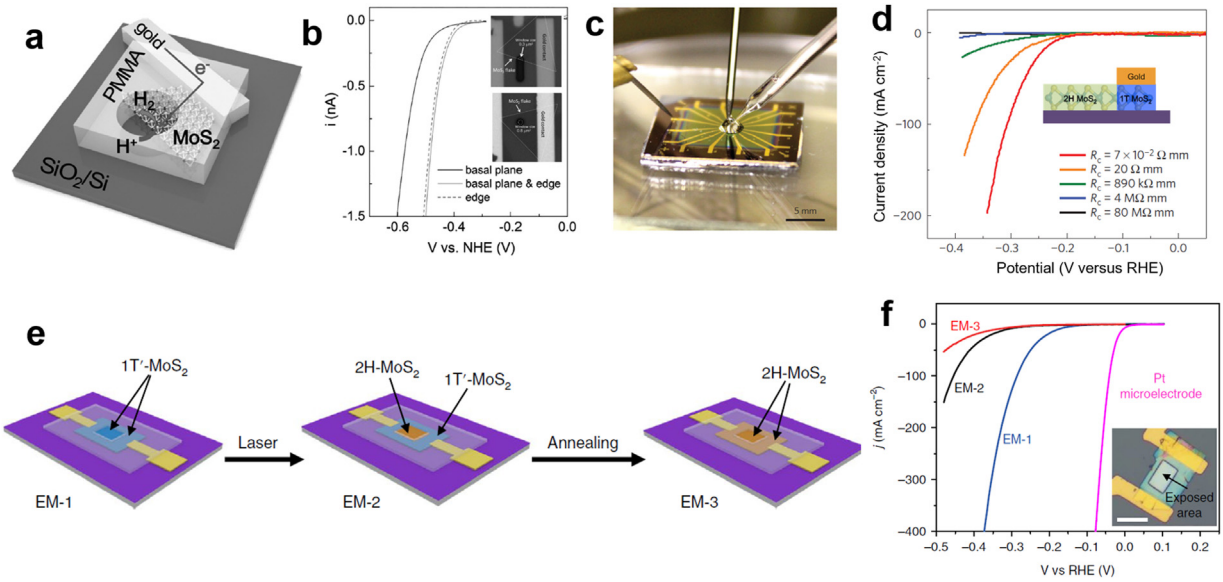

Fig. 7. (a) Schematic illustration of the on-chip local probe measurement setup. (b) Polarization curves of monolayer MoS_2 basal plane with and without edge active sites in HER. Inset: optical image of a MoS_2 flake with gold contact and HER window opened on the region containing both 0.3 μm^2 basal plane and 0.8 μm edge (upper)and the optical image of a MoS_2 flake with gold contact and HER window opened on basal plane (lower). The circular window size is about 0.8 μm^2. Reproduced with permission. [147] Copyright 2017, Wiley-VCH. (c) Photograph of the electrochemical microcell. (d) Polarization curves obtained from MoS_2 devices with various contact resistances from 80 MΩ mm down to 7×10^{-2} Ω mm. Inset: schematic of device with 1 T contacts and 2H basal planes. Reproduced with permission. [151] Copyright 2016, Nature Publishing Group. (e) Schematic of the fabrication of three types of electrochemical microcell (EM-1, EM-2 and EM-3). (f) Polarization curves obtained with EM-1, EM-2 and EM-3. Inset: optical microscope image of EM-1. Scale bar, 20 μm. Reproduced with permission [152]. Copyright 2018, Nature Publishing Group.

excellent catalytic performance. These results fully demonstrate that reducing contact resistance and enhancing charge injection can promote a catalytic hydrogen evolution reaction. Recently, the Zhang Group also demonstrated that the metallic phase can reduce contact resistance, which will greatly affect HER performance. [152] Specifically, they used laser irradiation to convert the localized 1 T' MoS_2 to 2H MoS_2, while the phase of MoS_2 in different regions can be controlled (Fig. 7e). Moreover, after an annealing treatment, the 1 T' region can be *in-situ* converted back to the 2H phase. This treatment facilitates reliable comparison of HER performance during the 2H and 1 T' phases (Fig. 7f).

In addition to the phase engineering of the contact, the electric field can also be used to tune electron injection. [153–156] Silicon wafer-based devices are widely used for field-effect transistor (FET) research on ultra-thin nanosheet [45,157,158]. Such FET-like devices are suitable for the field-tuned electrochemical reaction. In these on-chip devices, SiO_2 or another insulating oxide serves as the dielectric layer (gate) and electrons are injected from metal micro-electrodes (Fig. 8a). In 2016, Cummins et al. reported the first electric-field-tuned HER. [159] They reported the improved conductance of MoS_2 nanosheets showed obvious improvement. Almost simultaneously, the Mai Group described a similar gate-tuned HER device involving the design of a detailed experiment to verify the effect of electrical field on the HER performance of MoS_2 [160]. Interestingly, the positive gate voltage exerted a stimulating effect on the MoS_2 nanosheet, which demonstrated a dramatic decrease of overpotential as well as Tafel slope (Fig. 8b). For the optimal example, the overpotential decreased to less than 50 mV, which is nearly close to the performance of Pt. It must be noted, however, that Tafel slope did not reach a similarly small value, which may indicate that the reaction path cannot be optimized by the application of an electrical field. It is worth pointing out that an electric field will not only affect the distribution of electrons, but also the charged ions. Hence, the reaction kinetics can be tuned if ion distribution can be controlled. The researchers also reported the field effect tuned HER performance of VSe_2 nanosheet, [161] which is a metallic material and its conductance will not be affected by an electric field. This work separated the influence of ions and electrons, and the concentrated hydrogen ions show great enhancement of adsorption dynamics (Fig. 8c). Afterwards, they combined the electric field with illumination, which demonstrated the coupled enhancement of HER performance of MoS_2 [162]. Most recently, the Liu group reported self-gating phenomenon in semiconductor electrocatalysis [163]. Four different types of devices are fabricated, in-situ electronic/electrochemical measurement, thickness-dependent electrochemical measurement, top and bottom contact measurement, photoelectrochemical measurement are realized in an individual nanosheet to detect the semiconductor-electrolyte interface. They found that semiconductor electrode is modulated by electrochemical potential and presents insulating state or conductive states during electrochemical reaction, which accounts for the high performance in ultrathin semiconductors. Meanwhile, due to the complex electron transport mechanisms of nanosheets, many detailed issues must be addressed to identify the contribution from each factors. Zhou et al. designed individual MoS_2 and WTe_2 nanosheet devices with different contact configurations to separate different factors [164]. For instance, they compared two different contacts, MoS_2 with graphene contact and MoS_2/graphene heterostructure (show in Fig. 8d,e). The difference between these two cases is that the injection of electrons passes through in different ways. The former case achieved lower overpotential and the Tafel slope, which shows that the path for electron transport plays a vital role when the hydrogen adsorption energy and contact resistance remain the same (Fig. 8f).

Besides the hydrogen evolution reaction, on-chip devices were also applied in the research on the oxygen evolution reaction [62,165] and oxygen reduction reaction [166]. *In situ* monitoring the electrochemical surface state is supposed as an efficient method to uncover the mechanism of catalysis. To realize the *in situ* monitoring, researchers designed special circuits (Fig. 8g,h), namely *in situ* electrical transport spectroscopy (ETS) measurement. Under an electrochemical condition in aqueous, the adsorbed water molecules and hydroxyl species will form scatter centers. Hence, the variation of the resistivity can reflect the adsorption

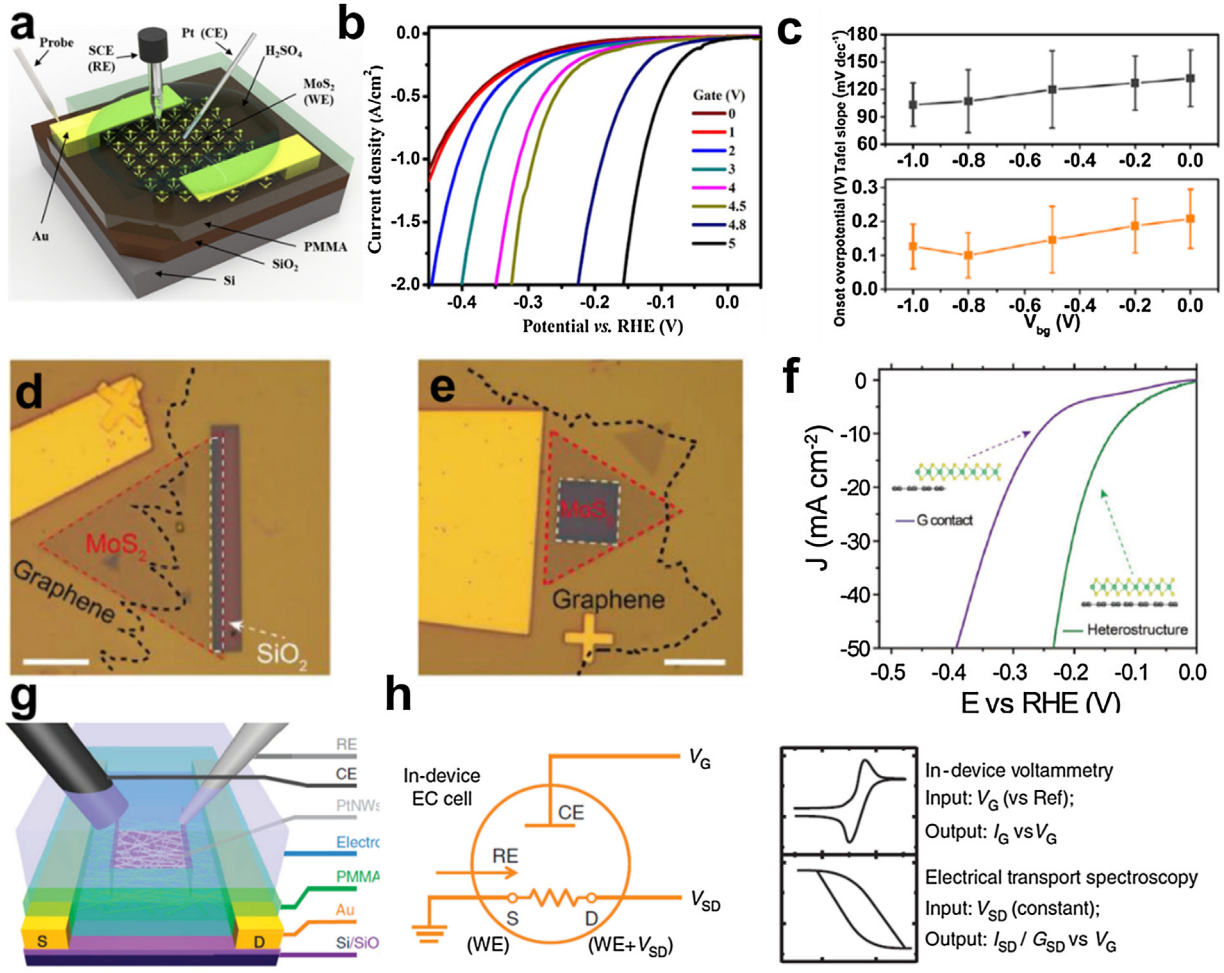

Fig. 8. (a) The schematic diagram of three electrodes for HER catalytic measurement. (b) The polarization curves of HER at different back gate voltages. Reproduced with permission. [160] Copyright 2018, Wiley-VCH. (c) Statistic-based influence of the back gate on the onset overpotential and Tafel slope. Reproduced with permission [161]. Copyright 2017, American Chemical Society. (d) Optical image of MoS_2 with a graphene contact with MoS_2 edge exposed, (e) Optical image of graphene/MoS_2 heterostructure with MoS_2 basal plane exposed. Scale bar, 10 μm. (f) Normalized polarization curves measured from the basal plane of the MoS_2 nanoflake device with a graphene contact, and of the MoS_2/graphene heterostructure. Reproduced with permission. [164] Copyright 2018, Wiley-VCH. (g) Schematic illustration of the platinum nanowire (PtNW) device with a microscopic electrochemical (EC) cell on it. (h) Schematic diagram of concurrent in-device CV and ETS for *in situ* monitoring of the electrochemical interfaces. CE, counter electrode; RE, reference electrode; WE, working electrode; S, source; D, drain. Reproduced with permission from ref. [165] (Copyright 2015, Nature Publishing Group).

state during potential scanning. It is also demonstrated that the metal nanomaterials are suitable for this measurement, because liquid gate potential cannot modulate the conductivity of metal material and the surface scattering contributes to the dominate signal. In recent work, platinum and nickel nanomaterials were systematically investigated, which shew great sensitivity to a typical electrochemical interface state. [62,165] In micro/nano devices, the conductivity of nanomaterials can be measured simultaneously. This advantage gives great opportunity for the *in situ* monitoring of the electrochemical reaction.

Energy storage devices

Electricity is a common natural phenomenon that is generated by the flow of electrons. In nature, lightning is a sudden electrostatic discharge process that generates a huge electrical spike. Nevertheless, the electricity from a lightning storm cannot be used because it cannot be stored. In the 18th century, the first Leyden jar was invented which was a milestone for electrical energy storage. In fact, Benjamin Franklin used Leyden jars to catch lightning in his famous "kite flying" experiments. With the development of a range of electrical energy storage (EES) technologies since the days of the Leyden jar, EES is becoming increasingly important for today's power generation needs.

There are many promising energy storage technologies, such as mechanical energy storage, [167] chemical energy storage [11,168], thermal energy storage [169] and electrostatic/magnetic energy storage [170]. Among these technologies, chemical energy storage is perhaps the fastest developing one. For instance, metal ion batteries, represented by lithium-ion battery [171], have experienced significant developmental progress due to the high demand for portable electronic devices. Consider, for example, that the number of mobile phones worldwide was more than 7 billion in 2015. In order to satisfy this huge and growing market, plenty of researchers are devoted to developing high energy and power density energy storage devices that are more powerful, have longer service life, take less time to charge and are more space-effective.

One of the most important concerns in the development of high-performance electrode materials is the need to clarify the various mechanisms associated with energy storage and capacity fading. Hence, the advancement of the next-generation characterization methods is essential. On the one hand, on-chip nano devices are excellent tools for the *in situ* characterization of nanomaterials. In recent years, research targeting nano-device-based energy storage

Please cite this article in press as: X. Pan, et al., On-chip micro/nano devices for energy conversion and storage, Nano Today (xxxx), https://doi.org/10.1016/j.nantod.2019.100764

has helped to elucidate its mechanisms more fully. And on the other hand, rapid progress on portable and embedded micro devices has accelerated the development of micro-battery/capacitors. This demand increases the application potential for miniature energy storage devices. In this section, three kinds of micro/nano on-chip energy storage devices are introduced: single nanowire electrochemical devices, individual nanosheet electrochemical devices, and on-chip supercapacitors.

Single nanowire electrochemical devices

Nanowire electrode materials possess some unique characteristics—notably, anisotropic (axial/radical) electron transport and ion diffusion. [172] These materials also feature unique geometrical advantages for the assembly and *in-situ* characterization of energy storage devices. In light of these advantages, nanowire electrode materials afford a range of interesting opportunities for both theory and application research.

Despite the fact that researchers have tried many different methods for enhancing cycling performance, the capacity fading of energy storage devices remains a primary concern. [53,173] Generally, capacity fading is caused by structural destruction and induced high electron and ion transport resistance [174,175]. In order to reveal the intrinsic mechanisms associated with the capacity decay of nanowire energy storage devices, Mai et al. designed and assembled an all-solid-state single nanowire on-chip electrochemical device for the *in-situ* detection of charge and discharge processes (Fig. 9a). [50] For a single nanowire, two micro metal electrodes are linked to it, which enables basic electrical transport and electrochemical measurement. This measurement configuration excludes the influence of external conductive additives and binders and, instead, provides more specific results. The study of a single vanadium oxide nanowire as a working electrode shows that after a shallow discharge of 100 pA, the conductance of the nanowire decreases by 2 orders of magnitude (Fig. 9b,c). After shallow charging, the conductivity returns to its original level. This process indicates that the structure change of nanowires caused by the insertion and extraction of lithium ions is reversible in case of shallow charge and discharge. In contrast, the conductance and Raman spectra of a single silicon nanowire before and after a stronger charge-discharge cycle show that the structure of silicon nanowires will be irreversibly damaged during cycling (Fig. 9d,e). Based on the *in-situ* characterization platform of a single nanowire all-solid-state devices, a direct connection was established between electrical transport and structure, charge and discharge states, confirming that the capacity decay and the conductivity drop are induced by the structure damage of nanowire. This contributes to the scientific law of the capacity decay of nanowire energy storage devices.

Later, based on the alterable configuration of on-chip device, Xu et al. designed two nanowire electrochemical devices with different exposure states in order to study the transport mechanism of lithium/sodium ions in nanoscale electrode materials. [176] In these devices, $H_2V_3O_8$ nanowires were used as a cathode material, highly oriented pyrolytic graphite (HOPG) flakes were used as anode material, and $LiPF_6$ was used as electrolyte. Device 1 connected four electrodes to one nanowire and only the metal electrodes were covered with SU-8 photoresist; the other parts (*i.e.*, nanowire) were exposed to the electrolyte (Fig. 9f,g). When testing this device (wire the circuit to electrode 1), it was found that the conductance between the 1–2 segments decreased by 96.5%, while the 2–3 and 3–4 segments only experienced a decrease of 9.2% and 1.9%, respectively. The experimental results show that lithium ions will follow the shortest path during the intercalation process. Lithium ions preferentially intercalate from the radial direction near the electrodes, which supplies abundant electron sources. In device 2, the nanowires were only exposed at one end, and other parts were covered with SU-8 photoresist (Fig. 9h,i). When the electrode 1 was used as an electrochemical test electrode, lithium/sodium ions were only able to intercalate at the ends of the nanowires. The conductance of 1–2, 2–3 and 3–4 segments after lithium ions intercalation decreased by 3.5%, 5.6% and 11.6%, respectively. Due to the high migration rate of electrons along the nanowire axis, the low axial migration rate of lithium ions limited the electrochemical reaction. Eventually, the reduced structure damage and lower conductance drop can be achieved in the segments further away from the electron source. This well-designed single nanowire battery is highly appropriate for studying the basic reaction principles of nanowire electrode materials in an electrochemical reaction. Hou et al. also demonstrated similar ion transport characteristics. They used scanning photocurrent microscopy (SPCM) to detect ion transport in VO_2 nanowires. [177] Although it is not a standard electrochemical energy storage system, which is more like a liquid-gated field-effect transistor (Fig. 9j), this device provides a precise method for detecting ion transport. In this device, PMMA was used to cover the nanowire with only one side of the VO_2 nanowire exposed. The researchers were able to successfully visualize ion transport by SPCM and photocurrent mapping, which made it clear that ions were injected into the VO_2 nanowire and diffused along the axis (Fig. 9k).

Electrochemical test platforms based on a single nanowire can be used to detect certain optimization mechanisms and principles because they can accurately measure the electrochemical performance of single nanowire. [178] Hu et al. assembled three different single nanowire devices to investigate the optimized effect of graphene in energy storage system—namely, pure MnO_2, rGO (reduced graphene)/MnO_2 and pGO (porous graphene)/MnO_2 [179,180]. Electrochemical measurement results demonstrate that while a graphene scroll can significantly improve the conductance of MnO_2 nanowires, the graphene surface reduces the ion diffusion rate (Fig. 10a). Porous graphene can effectively solve this problem: it can produce a higher ion diffusion rate as well as increase conductance (Fig. 10b). For the rGO/MnO_2 nanowires, the ions can only transport from the gap between the graphene and the nanowires, while for the rGO/MnO_2 nanowires, the ions can transport from both the gap and the pores in graphene.

Liao et al. also used a similar approach for detecting the role that heterostructure plays in an electrochemical reaction. [181] As is known, constructing a nano-heterostructure is a common strategy for improving the performance of electrode materials (*e.g.*, improve structural stability and enhance electron transport). Although it is clear that the heterostructure modulates the electron transport and the ion transfer barrier at the interface, more in-depth mechanisms associated with this process were not discussed. And indeed, this goal would be difficult to achieve using a conventional battery configuration due to the mixed interfaces. Hence, the authors fabricated an on-chip device based on a MoS_2/MnO_2 heterostructure (Fig. 10c,d). Specifically, the MoS_2/MnO_2 heterostructure was fabricated by stacking a multilayer MoS_2 nanosheet and a MnO_2 nanowire forming a van der Waals (vdWs) heterostructure. They reported that measurements obtained from the MoS_2 and MnO_2 demonstrated different capacity and ionic-diffusion properties. *In-situ I–V* measurements indicate that unilateral conduction determined these distinct charge and discharge properties. This research provides a useful guide for the design of heterostructure electrode materials—principally, that heterostructure construction needs to follow the electrons transport path.

Individual nanosheet electrochemical devices

In addition to on-chip single nanowire electrochemical devices, there are some representative studies that have examined the role of individual nanosheet, such as MoS_2,[182] graphene [183] and

Please cite this article in press as: X. Pan, et al., On-chip micro/nano devices for energy conversion and storage, Nano Today (xxxx), https://doi.org/10.1016/j.nantod.2019.100764

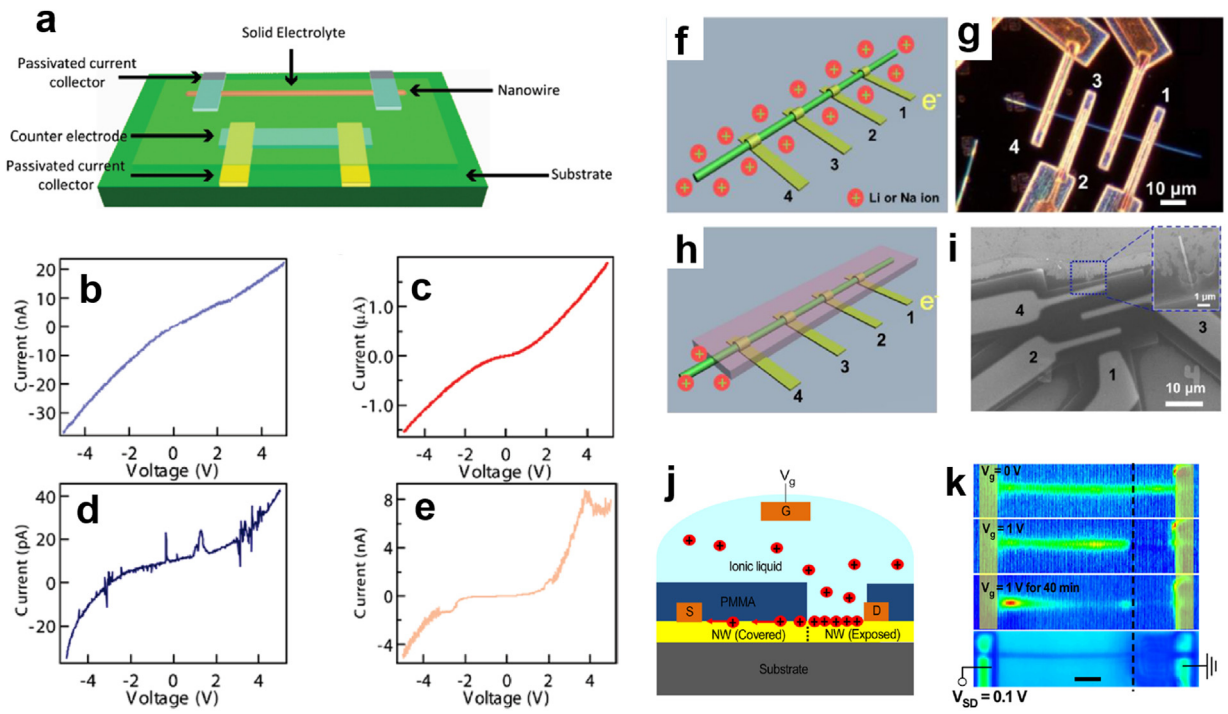

Fig. 9. (a) Schematic diagram of a single nanowire electrode device design. A single vanadium oxide nanowire or Si. (b–e) Single vanadium oxide nanowire transport properties at different charge/discharge states: (b) after Li^+ ion intercalation (shallow discharge with 100 pA for 200 s); (c) after Li^+ ion deintercalation (shallow charge with -100 pA for 200 s); (d) after deep discharge with 100 pA for 400 s; (e) after deep charge with -100 pA for 400 s. Reproduced with permission. [50] Copyright 2010, American Chemical Society. (f, g) Single nanowire device with the first configuration. (f) The first configuration, in which the nanowire is fully immersed in the electrolyte. (g) The dark field optical microscopic image of the nanowire electrode. (h,i) Single nanowire device with the second configuration. (h) The second configuration, in which the nanowire is covered by a passivation layer with only one exposed end. (i) The SEM image of the device with the second configuration. Only one end of the nanowire is exposed in the electrolyte (inset). Reproduced with permission [176]. Copyright 2015, American Chemical Society. (j) Schematic illustrating ion injection into the exposed NW and subsequent diffusion into the covered NW. S and D are source and drain metal contacts, respectively. (k) Photocurrent images at V_{SD} = 0.1 V taken at V_g = 0 V, immediately, and 40 min after V_g is increased to 1 V, respectively. Reproduced with permission. [177] Copyright 2017, American Chemical Society.

some other layered materials. Layered materials with a significant vdWs gap can usually serve as the host for ions [184,185]. When ions intercalate into layered materials, the physical and chemical properties will vary quite substantially [186]. These persistent issues demand further research into the *in situ* characterization of individual nanosheets.

In order to achieve successful *in-situ* optical observations, researchers have assembled transparent devices on a glass substrate instead of a silicon wafer. The Hu Group reported the fabrication of individual graphene and MoS_2 micro transparent battery devices in 2014 and 2015, respectively. [182,187] In these two *in-situ* research studies, the researchers were able to elucidate both electrical transport performance and optical property characteristics *via* electrochemical testing. Their devices were fabricated on a glass plate, and another glass plate was employed as a top sealing plate to assemble a transparent few-layer graphite/MoS_2 micro-battery, which can be combined with a probe station and an optical microscope to *in-situ* test the few-layer graphite and MoS_2 nanosheets. [187] Subsequently, *in situ* Raman spectra and transmittance were measured, enabling them to determine the *in situ* relationship between transmittance and discharge state. During the discharge process (shown in Fig. 11a,b), transmittance will undergo three stages of gradual increase, which becomes more obvious in a multilayer graphite. Simultaneously, electrical conductivity will also increase when Li^+ ions intercalate into graphite, which was also confirmed *via in situ* measurement based on the on-chip device.

In their work of MoS_2 microbattery, [182] Hu and coworkers fabricated a similar device on a glass substrate (Fig. 11c). Interestingly, they found that the discharge rate will greatly change the electrical conductivity of MoS_2. If the discharge process is rapid, resistance will decrease over three orders of magnitude. They attributed this phenomenon to the structure of final product, Mo and Li_2S. During a slow lithiation process, Mo will form isolated particles and the Li_2S will contribute to the increased resistance (Fig. 11d). In contrast, when the discharge process is fast, a linked network of Mo nanoparticles will form and the resistance will decrease substantially. These two studies provide an important methodology for *in situ* investigation of the relationship between structure evolution and electrochemical performance for nanomaterial during charge/discharge process. In particular, they confirmed that reliable *in situ* measurements can be obtained more easily rather than having to rely on high vacuum in transmission electron microscopy (TEM). The Cui Group also described similar work with a MoS_2 on-chip device. [188] They recorded the intercalation process of Li ion using a digital camera, which demonstrated interesting results: that Li ion intercalation will follow a path from the edge to center of the MoS_2 nanosheet.

Based on the many advantages of *in situ* characterization methods, an on-chip device can play an important role of detecting the complex dynamics associated with ion transport. While the studies described earlier have qualitatively detailed ion transport in nanowire/nanosheet by *in situ* on-chip characterization, the challenge remains in determining how to accurately obtain reliable quantitative measurement. Accordingly, the use of ultrathin nanosheets may provide an avenue for obtaining quantitative measurements. Kühne et al. used an on-chip device (Fig. 11e,f) to detect the Li ion diffusion characteristics in bilayer graphene. [183] Given that electronic transport is a common criteria for the state of lithiation of electrode materials, Hall voltage can be measured simultaneously in order to obtain the Li density of different locations. According to Fick's second law for one dimen-

Please cite this article in press as: X. Pan, et al., On-chip micro/nano devices for energy conversion and storage, Nano Today (xxxx), https://doi.org/10.1016/j.nantod.2019.100764

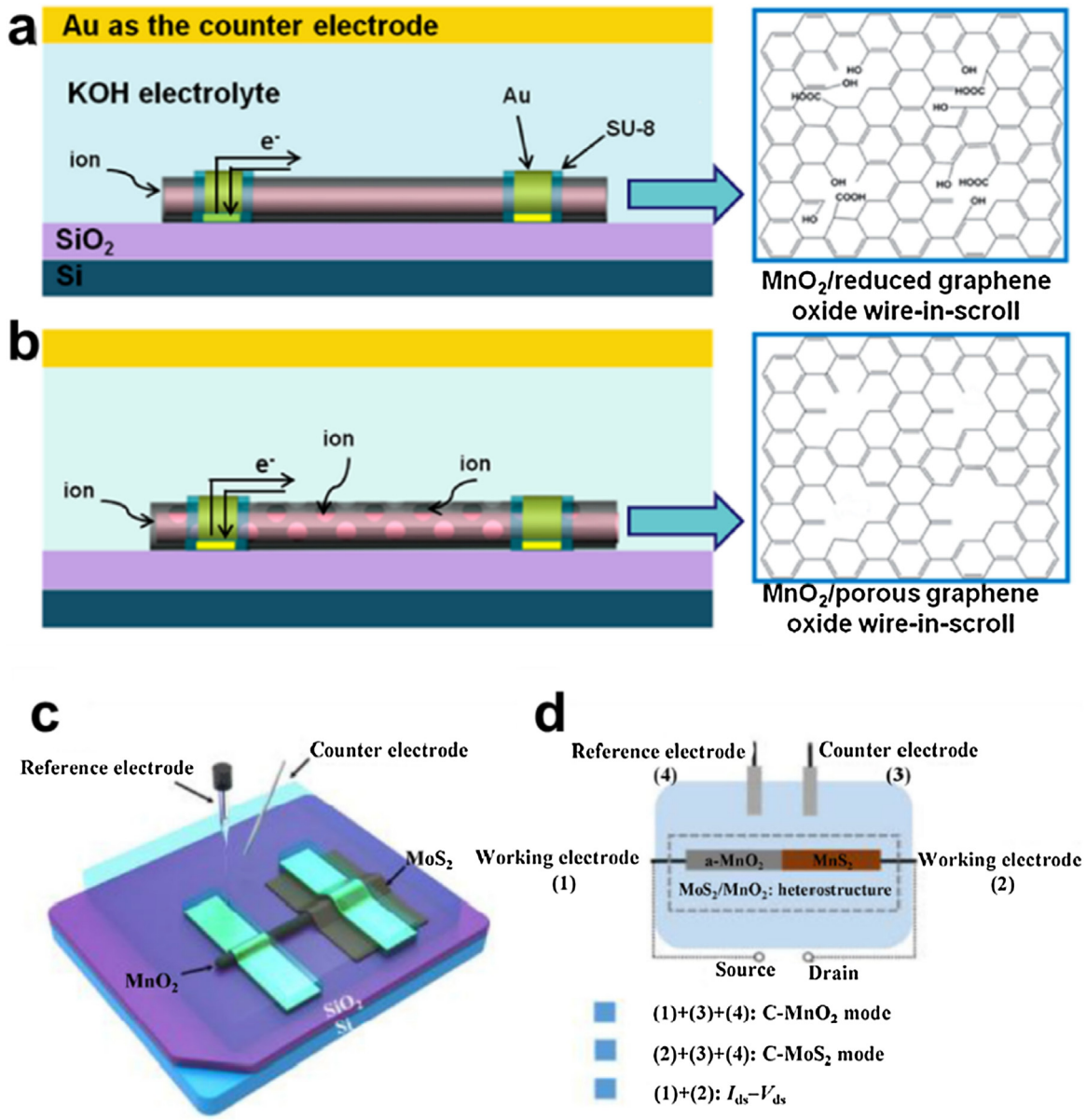

Fig. 10. (a) Schematic illustration of a MnO_2/rGO NW device and reduced graphene oxide. Ion transport only through the gap between the graphene and the MnO_2 NW. (b) Schematic illustration of a MnO_2/pGO NW device and porous graphene oxide. Ion transport through not only the gap between the graphene and the MnO_2 NW but also the pores in the graphene. Reproduced with permission. [179] Copyright 2016, American Chemical Society. (c) Schematic illustration of the MoS_2/MnO_2 heterostructured energy storage device. Two working electrodes (1) and (2) are separately connected to the layered MoS_2 nanosheet and single MnO_2 nanowire. Ag/AgCl and a Pt wire serve as reference electrode (4) and counter electrode (3), respectively. A 6 M KOH solution is used as the electrolyte. (d) Illustration of the testing modes for the MoS_2/MnO_2 heterostructured energy storage device. Reproduced with permission. [181] Copyright 2017, Tsinghua University Press and Springer-Verlag GmbH Germany.

sional case, $\frac{\partial n_{Li}}{\partial t} = D^{\delta}\frac{\partial^2 n_{Li}}{\partial x^2}$, for ascertaining the diffusion coefficient, two functions are needed: time-dependent and length-dependent Li density. The infinite length and well-confined device offer both time- and location-boundary condition. They disclosed that the in-plane chemical diffusion coefficient of Li can go up to $D^{\delta} = 7 \times 10^{-5}\ cm^2\ s^{-1}$. This quantitative work proved that the combination of electrochemical methods, magneto-transport tools, and on-chip device is a powerful tool for characterizing ion transport in low-dimensional systems. In the most recent work, they reported the observation of super dense of lithium atoms in bilayer graphene, which is assumed as a multi-layered close-packed order. [189] They combined the aforementioned device with low-voltage transmission electron microscopy and realized the *in situ* observation of lithium atoms in bilayer graphene. These two works are important progress in on-chip micro/nano device which show a promising direction for on-chip device. The quantitative research and *in situ* observation of ion transportation will become the key point in developing on-chip energy storage devices.

On-chip micro-supercapacitors

With the rapid development of miniturized electronic devices (including flexible electronic devices), the demand for cost-effective micro energy storage devices is also increasing. [190] Accordingly, studies addressing the development, characterization, performance, and application of micro energy storage device are expanding. In the following subsection, we introduce micro-supercapacitors (MSCs) as an example of micro-energy storage devices and the ongoing research progress surrounding these devices [191,192]. Micro capacitors are an indispensable elec-

Table 2
Summary of the performance and the micro-fabrication process of interdigital MSCs.

Fabrication method	Specific capacitance (mF cm^{-2})	Power density (mW cm^{-2})	Rate performance	Interspace (μm)	Asymmetric(Y/N)	Electrode materials	Highlights	Ref.
3D printing	207.9	3.77	58.3% (0.63 to 4.71 mA cm^{-2})	1000	Y	V_2O_5/GO/graphene-vanadium nitride quantum dots	Ultrahigh areal energy density	[207]
Brush coating	153.34	0.44	58.7% (10 to 100 mV s^{-1})*	1000	N	porous carbon	Biodegradable	[208]
Stamping	61	0.33	95.6% (10 to 100 mV s^{-1})*	550	N	MXene	Advanced fabrication process	[209]
Electrochemical deposition	52.9	13.8	58% (10 to 100 mV s^{-1})	100	N	MnO_2	Printable fabrication	[210]
Laser-assisted etching	40	5.4	79.5% (10 to 100 mV s^{-1})*	26	N	graphene	Precisely geometry controlled	[211]
Laser-assisted etching	34.6	0.18	23.1% (1 to 100 mV s^{-1})*	1000	N	MXene/graphene	Self-healing	[212]
Screen printing	25.8	7.32	11.8% (0.305 to 9.76 mA s^{-1})	396	N	MnO_2	Multifunctional intergration	[213]
Laser-assisted etching	22.09	2.34*	49.0% (0.6 to 17.5 A cm^{-3})*	300	N	Ppy/graphene	Flexible	[214]
Laser-assisted etching	21.8	1.765	63.9% (2 to 100 mV s^{-1})*	150	Y	CNTs/MnO_2	Large-scale fabrication	[215]
Mask-assisted filtration	21	0.925*	42.9% (0.2 to 2.0 mA cm^{-2})*	500	Y	VN, $Co(OH)_2$	Voltage of windows: 1.5 V	[216]
Mask-assisted filtration	17.4	15	64.3% (1 to 100 mV s^{-1})*	500	N	graphene	Scalable production	[217]
Mask-assisted filtration	9.8	–	34.7% (5 to 100 mV s^{-1})*	500	N	phosphorene/graphene	One-step device fabrication	[195]
Electrochemical deposition	8.15	0.0249*	70% (20 to 200 mV s^{-1})	400	N	Ppy	Durable, transferable	[218]
Lithography	5.9	1.014	–	10	N	carbon	Pore-Patterned constructioin	[219]
Electrochemical deposition	1.83	–	–	50	N	PEDOT	Thermoswitchable	[220]
Inkjet printing	0.7	–	68.5% (10 to 100 mV s^{-1})*	200	N	graphene	Scalable fabrication	[221]
Inkjet printing	0.26	0.00195*	54.1% (0.005 to 0.02 mA cm^{-2})*	2	N	δ-MnO_2	High precision	[222]
Preset filling	0.249	–	32.1% (5 to 100 mV s^{-1})*	1000	N	CNTs	Multifunctional intergration	[223]
Laser-assisted etching	0.0627	32	96.8% (10 to 100 mV s^{-1})*	100	N	graphene	Ultrahigh power output	[224]
Nanoimprint lithography	0.008	0.054*	37.6% (2 to 100 mV s^{-1})*	0.5	N	carbon	High precision	[225]

* These data were calculated by the authors.

Please cite this article in press as: X. Pan, et al., On-chip micro/nano devices for energy conversion and storage, Nano Today (xxxx), https://doi.org/10.1016/j.nantod.2019.100764

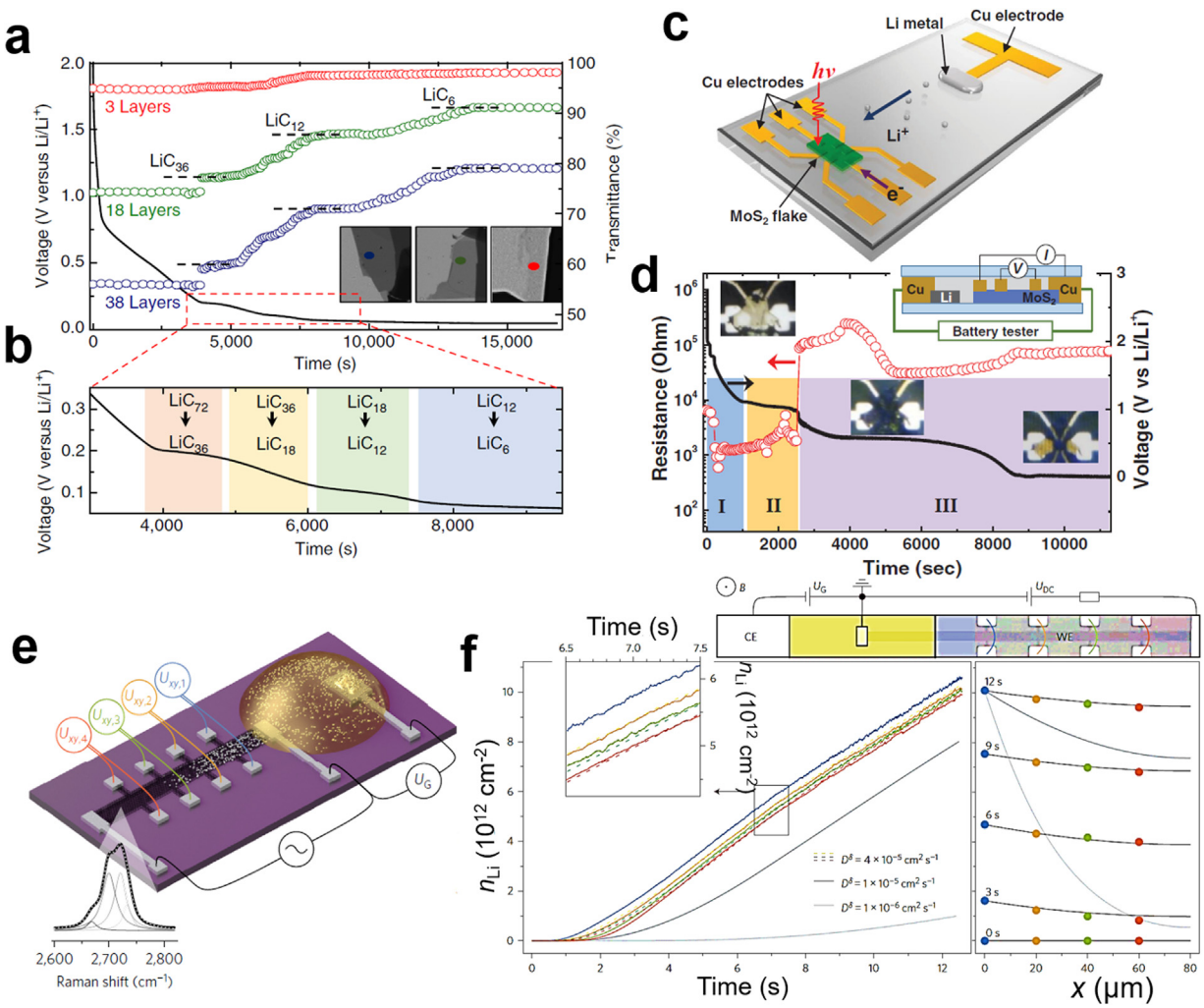

Fig. 11. (a) Optical transmittance (right) and electrochemical potential (left) *versus* lithiation time are plotted. (b) Detail of voltage profile *versus* time near the intercalation plateau. Reproduced with permission. [187] Copyright 2014, Nature Publishing Group. (c) Schematic of MoS_2-Li microbattery. (d) Resistance *versus* time of MoS_2 flake undergoing electrochemical lithiation at constant current. Insets show a schematic of the microbattery setup for *in situ* resistance measurement (upper right), and optical images of lithiated MoS_2 at stages I, II, and III, from left to right. Reproduced with permission. [182] Copyright 2015, Wiley-VCH. (e) Schematic of the device (not to scale). Bilayer graphene is etched into a Hall bar geometry. The electrodes either enable electronic transport measurements or serve as a CE to control the lithiation. The inset shows the characteristic four-component Raman scattering response of bilayer graphene (intensity in arbitrary units), measured for an excitation wavelength λ =488 nm. (f) Direct measurement of Li diffusion. The schematic (top) of the Li$^+$ (CE)|electrolyte (yellow shaded area)|$C_6Li_{2y}C_6$ (WE) cell includes an optical micrograph of the uncovered bilayer graphene area with probes used for the Hall measurements. The Hall probe pairs are marked in the same colour as the corresponding data set in the panels below. Left panel: Li concentration n_{Li} extracted from Hall measurements at B = 10 T and T =300 K as a function of time at four positions along the bilayer graphene device (blue, yellow, green and red). The dashed lines of slightly different colours are solutions to equation (3) for $D^\delta = 4 \times 10^{-5}$ cm^2 s^{-1} as explained in the text. Solutions for lower values of D^δ are shown as grey lines. The inset is a magnification at around t = 7 s. Right panel: Li density profiles across the bilayer at different times (black lines), with measured values shown as coloured dots. The grey lines show the density profile for the same lower D^δ values as in the left panel. Reproduced with permission. [183] Copyright 2017, Nature Publishing Group.

tronic component used in integrated circuitry. With the rapid development of circuit integration technology, the manufacturing technology of circuit functional capacitors represented by metal-plate capacitors is also advancing [14,190]. As an energy storage module, supercapacitors have been combined with a battery to form a hybrid module for various power-output devices [193]. Therefore, MSCs function as a basic functional capacitor element or an energy storage module element (or both) in a microelectronic device [194]. When researchers fabricate MSCs by micro/nano processing technologies, power density and energy density represent two important performance indicators that must be considered. From a research perspective, the materials and device manufacturing processes of MSCs are mutually dependent. Therefore, in comparison with supercapacitors that have fewer design and fabrication considerations, MSCs have higher requirements for electrode materials and device fabrication process that then inform key performance characteristics. Additionally, the projected size of a micro device is entirely dependent on the fabrication process, after which its properties must be thoroughly evaluated before it can enter the commercial market. The other interesting and efficient MSCs conducted with innovative fabrication process are also needed to be commented. Han et al. fabricated a phosphorene/graphene-based MSC with high energy density *via* vacuum filtration, which is known as one step. [195] Generally, filtration for thin-film fabrication as electrode is the general method. Interestingly, as shown in Table 2, the larger interspace mainly corresponds to higher specific areal capacitance. Combining with the analysis about the areal mass loading, we find that large interspace could enhance the stability of MSC even in higher mass loading. However, some researchers ignored the area of interspace and just calculated the areal specific capacitance according to the utilized area. In the MSC with large interspace, the ion diffusion path and

Please cite this article in press as: X. Pan, et al., On-chip micro/nano devices for energy conversion and storage, Nano Today (xxxx), https://doi.org/10.1016/j.nantod.2019.100764

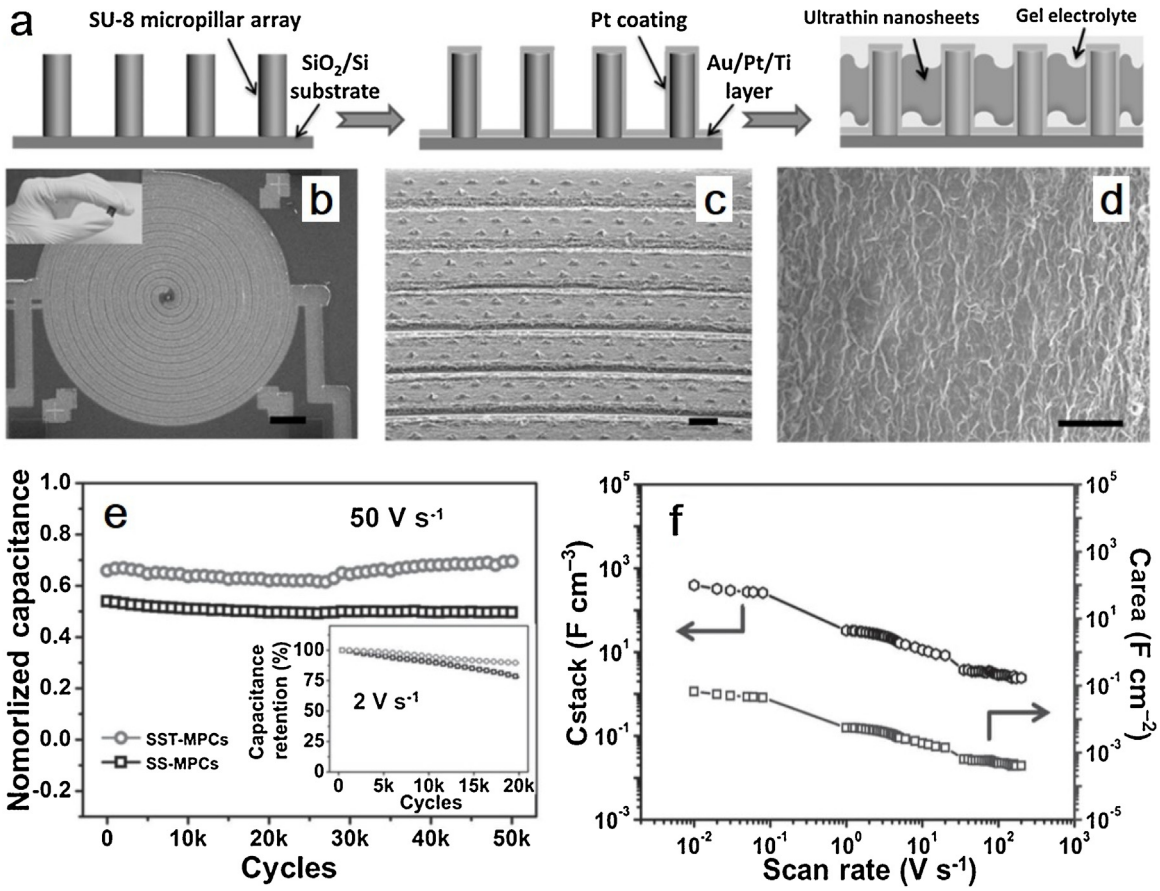

Fig. 12. (a) Schematic illustration of the fabrication process of all-solid-state spiral-shaped three-dimensional micropseudocapacitors (SST-MPCs). (b–d) SEM images of SST-MPCs. The inset in (b) shows the optical image of SST-MPCs. (e) Cycling stability of SST-MPCs and SS-MPCs at the scan rate of 50 V s^{-1} over 50,000 cycles, where SST-MPCs show the excellent stability and much higher capacitance compared with SS-MPCs. The inset in (e) represents the capacitance retention of SS-MPCs and SSTMPCs at the scan rate of 2 V s^{-1} for 20,000 charge-discharge cycles. (f) Evolution of the stack/areal capacitance at different scan rates of SST-MPCs. Scale bars: (b) 200, (c) 10, and (d) 5 μm. Reproduced with permission. [72] Copyright 2015, Wiley-VCH.

charge transfer resistance does not change obviously. However, the limited area of device means that all area of device including the interspace should be considered during the relative calculation. Thus, the interspace and the construction of electrode should be highlighted especially for the choice and the design of microfabrication process.

The Mai Group described a technique that combined photolithography and electrochemical deposition to achieve ultra-high power density and energy density of MSCs (Fig. 12). [72] The intent of incorporating these two processes is to improve MSC mass-loading and the effective electronic transmission path (*i.e.*, the current collector) under conditions of device stability and micromachining accuracy. This work utilized electron beam lithography technology and physical vapor deposition (PVD) to build in-plane collectors as the main circuit for electronic conduction, as shown in Fig. 12a-d. In order to give full play to the space characteristics of the device, a three-dimensional cylinder was designed out of the plane to eliminate the problem of a single active material mass-loading in the plane; that is, the increase in mass-loading is the key to improving energy density. On the other hand, due to the electrochemical deposition process, the real areal mass-loading was kept at a relatively low level, which served to decease the electron transport distance within the active material of the electrode, as well as promoting the fast and efficient electronic conduction of the entire device, thus ensuring excellent rate performance (Fig. 12e,f). This type of MSC represents the typical fabrication method used at present, while also incorporating more mature microfabrication technologies. Lin et al. also conducted an electrochemical deposition study—not only three-dimensional current collector, but also to simplify the process and increase the operability of the process. [196] By controlling the electric signal input in the electrochemical deposition process, a tree-like nickel-based current collector was constructed, and the in-plane area of the MSCs was fully utilized (Fig. 13a). As shown in Fig. 13b,c, it is noteworthy that in the process of electrodepositing nickel, the potential distribution in the interdigitated gold current collector was not uniform. As such, it formed a varying degree of deposition from the middle part to the edge, which limited processing-accuracy improvements to some extent. However, the gap between the positive and negative electrodes is ten micrometers, which is very competitive. The relative electrochemical performance of tree-like nickel-based MSC, shown in Fig. 13d,e, also confirmed that the 3D current collector for MSC is very efficient at improving the rate performance and specific capacitance.

It should also be noted that the size of an MSC is an important factor for determining its processing parameters (*i.e.*, using a segmentary approach or not). Indeed, the laboratory production of MSCs have been restricted by nonstandard automachinery—meaning that current manufacturing processes and the controllability of fabrication processes/precision leave a lot of room for optimization. Another design criterion is whether the fabricated process could compatible with various electrode materials like MXene (which is difficult for electrochemical deposition, but appropriate for inject-print, filtration, and so on), and graphene (restacking will limit the structure construction and ion transport). Thus, more varied and efficient ways of combining with novel

Please cite this article in press as: X. Pan, et al., On-chip micro/nano devices for energy conversion and storage, Nano Today (xxxx), https://doi.org/10.1016/j.nantod.2019.100764

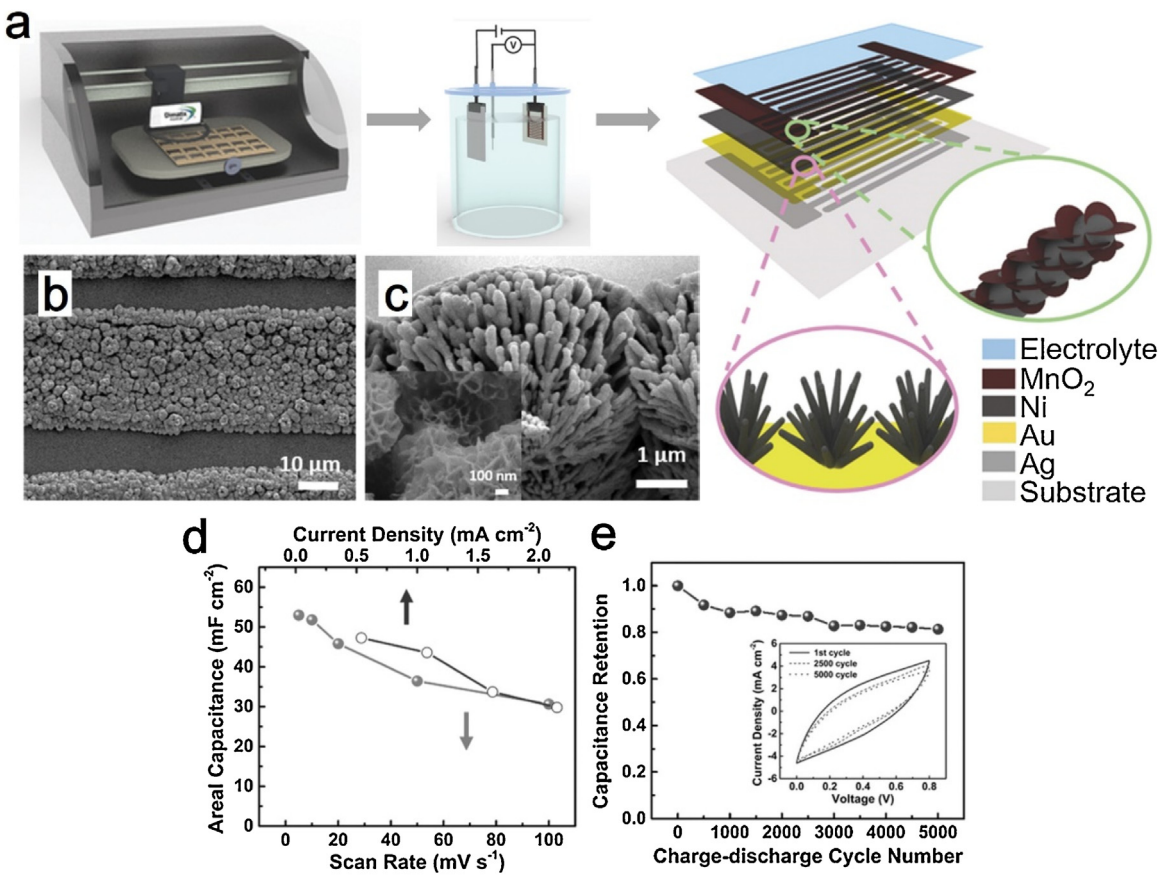

Fig. 13. (a) Schematic illustration of the printable fabrication procedure. (b,c) SEM images of MnO_2 nanoflakes on Ni nanocoral (Ni@MnO_2). Inset in (c) is the inset are high-magnification images. (d) Areal capacitances of device with optimized MnO_2 mass loading calculated from CV and GCD measurements, respectively. (e) The cycling stability test of the device at a scan rate of 100 mV s^{-1}. Inset: CV curves at the first cycle, after 2500 and 5000 cycles. Reproduced with permission. [196] Copyright 2017, Wiley-VCH.

microfabrication and related properties for achieving active electrode materials need further investigation.

Xiao et al. fabricated phosphorene/graphene-based MSC with relatively high energy density using interdigital template filtration—which is known as one-step fabrication, as shown in Fig. 14a. [195] While filtration for thin-film electrodes has been widely explored (*e.g.*, in works pertaining to the application of flexible electrodes in lithium ion battery), this is not the case with MSCs. Given their novel paths for material assembly, coupled with the fact that the processes used for the generation of thin-film electrodes for supercapacitors or metal ion batteries could also extend to MSCs, this means that more types of materials (*e.g.*, pseudo-capacitance and ion-capacitance materials) may also play a role in the fabrication of graphene-based MSCs. Indeed, Bao and coworkers reported a series of filter-extraction assembly and material optimization approaches for improving the performance of MSC. Graphene and phosphorene, as two-dimensional capacitance materials storing energy by electric double-layer capacitor, were used to fabricate symmetric MSC. This effort represents the first time that phosphorene was used in fabricating an MSC that delivered high energy density (11.6 mW h cm^{-3}), which the researchers attributed to film manufacturing and optimization for structural integration of both graphene and phosphorene (Fig. 14a) [195]. To highlight the superiority of this fabrication process, an asymmetric MSC based on 2D VN nanosheets and $Co(OH)_2$ nanoflowers was also assembled successfully, achieving 12.4 mW h cm^{-3} volumetric energy density (Fig. 14b) [197]. Thus, the lithium ion capacitance material (carbon-coated $Li_4Ti_5O_{12}$) was applied an a hybrid MSC, delivered 53.5 mW h cm^{-3} volumetric energy density (Fig. 14c) [198].

Carbon micro-electro mechanical systems (C-MEMS) represent another method that can deliver higher processing accuracy. In recent years, this technology has been widely used in miniature energy storage devices and miniature sensor devices. Compared to other methods, C-MEMS is more suitable for micro/nano processing and micro-device assembly. Based on the characteristics of this process and the characteristics of micro-supercapacitors, the Mai Group designed various materials/carbon composite-layered structures and carbon nanotubes [199–201]. The researchers showed that the structure of the carbon/carbon composite structure could be improved along a certain volume range from specific capacity enhancement, electron transport, and the like. Herein, differing from the fundamental consideration of single nanowire/sheet device, the application-oriented miniature device highlights the stability and the device-architecture design limited by limited space. The synergic relationship between choice of electrode materials, structure of current collector and architecture of device should be evaluated, especially for new micro-fabrication process. The space utilization (the stacking of electrode materials) and effective occupied area of electrode materials are another two fundamental consideration.

Conclusion and outlook for future research

The related areas of nanotechnology and nanomaterials hold great promise for the development of advanced energy technologies. On the downside, scientists and engineers are still grappling with effective ways of determining their basic properties and processing properties. Accordingly, micro/nano devices can play a vital

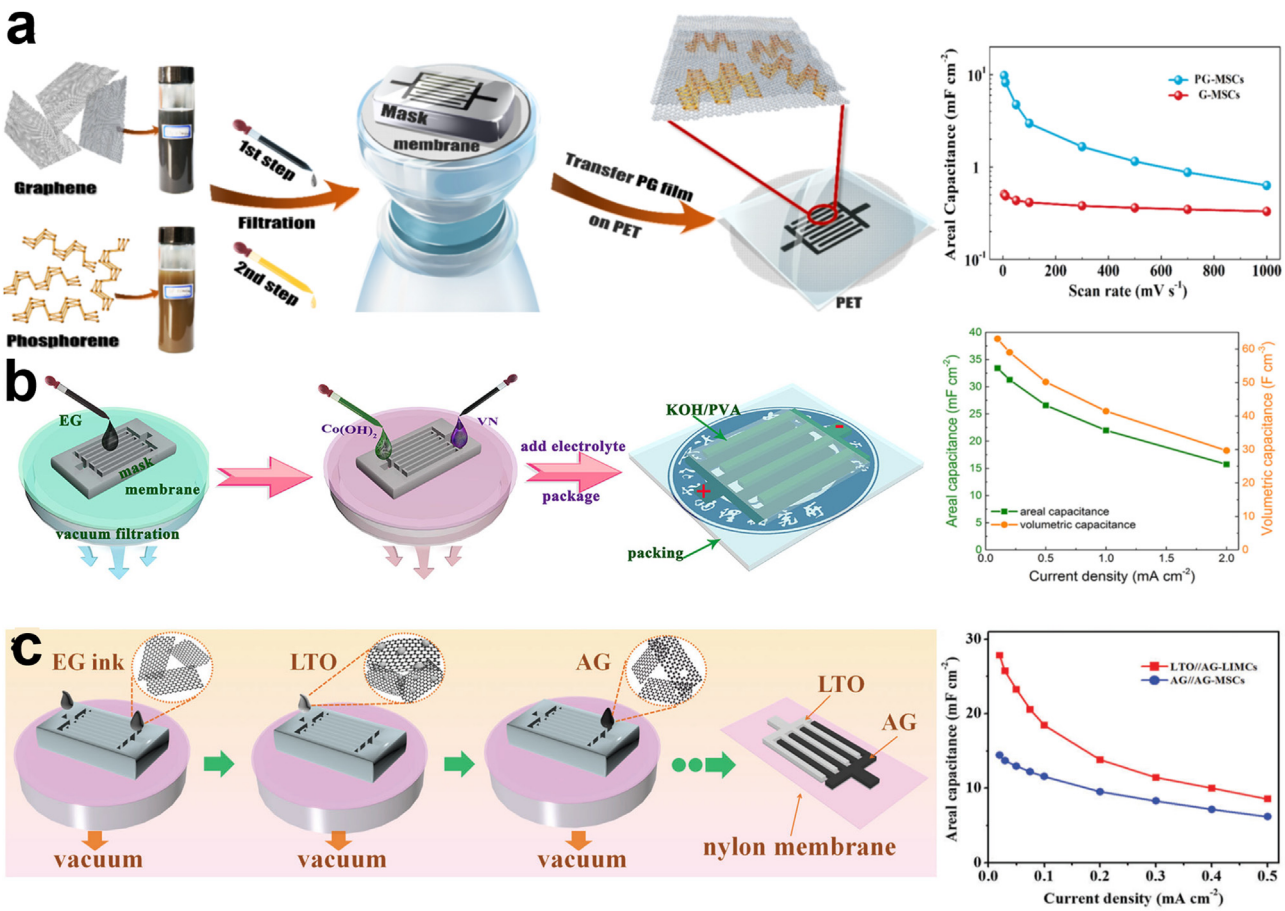

Fig. 14. (a) Schematic illustration and specific capacitance at different rate of phosphorene and graphene interdigital MSCs. Reproduced with permission. [195] Copyright 2017, American Chemical Society. (b) Schematic illustration and specific capacitance at different rate of 2D VN nanosheets and $Co(OH)_2$ planar hybrid MSCs. Reproduced with permission. [197] Copyright 2018, Nature Publishing Group. (c) Schematic illustration and specific capacitance at different rate of lithium ion MSCs. Reproduced with permission. [198] Copyright 2018, The Royal Society of Chemistry.

role in assessing the physical and chemical properties of individual nanomaterial. Moreover, on-chip micro/nano devices are becoming increasingly effective for use in *in-situ* monitoring and diagnosis using one or more different characterization methods, *e.g.*, Raman and photoluminescence spectra, scanning photocurrent microscopy and *in situ I–V*.

In this review, some of advanced applications of on-chip micro/nano devices are introduced. A growing body of intriguing research based on on-chip devices has elucidated a range of important principles and properties, *e.g.*, the photoelectric conversion efficiency of single nanowire, and the electrochemical measurement of MoS_2 edge and planar regions. These results simply would not be possible using macro-sized devices. Based on the specific performance requirement, researchers have designed different types of novel devices, such as lying or standing nanowire devices; multi-contact and even integrated devices; a single nanomaterial device, and heterostructural devices. Additionally, characterization methods are also experiencing rapid advances, which is essential for the development of electrochemical energy storage devices because *in-situ* monitoring is very difficult (if not impossible) for tradition batteries and capacitors. Instead, the use of on-chip devices makes it significantly easier to focus on one individual nanomaterial or specific region, thereby achieve accurate *in situ* assessments. Moreover, on-chip micro/nano devices with high energy conversion efficiencies also hold great promise for use in nanoscale energy harvesting. In an era of exploding information technologies, consumer demands mean that devices are becoming smaller and smaller.

What is the future of micro/nano energy conversion and storage devices? There are three possible promising scenarios. First, the architecture of on-chip devices will be more sophisticated for object-oriented design, simulating more complex physical and chemical models. The main merit of on-chip device is that the dimension of real functional component/reaction interface is reduced to 2D and 1D and electrodes are organized in plane, while in conventional devices are stacked. This point endows two kinds of great convenience, introducing more physical fields in typical orientations to tune degrees of freedom and constructing 3D micro/nano structure. To this point, multi-physics filed coupling can be introduced to uncover the basic reaction mechanism and transport model in a complex artificial nanostructure. Besides, it can be expected that more fields of energy technologies (*e.g.*, artificial photosynthesis) will be explored by the on-chip devices based on the rapid developing micro-electro mechanical system (MEMS) technologies. Second, the combination of on-chip device and high-resolution characterization technologies will play an increasingly important role. Nowadays, some spectrum technologies can be used with on-chip devices, *e.g.*, Raman spectrum. In the future, however, we expect that more powerful tools will be combined to advance the potential of on-chip devices, such as TERS (tip-enhanced Raman spectroscopy) and XPS (X-ray photoelectron spectroscopy). These new characterization methods will broaden the application of micro/nano devices and give significant structural and chemical information in micro probe analysis. For instance, next-generation nanodevices are likely to broaden the research horizons for heterostructures (*e.g.*, van der Waals het-

Please cite this article in press as: X. Pan, et al., On-chip micro/nano devices for energy conversion and storage, Nano Today (xxxx), https://doi.org/10.1016/j.nantod.2019.100764

erostructure and lateral heterojunction) and the other complex structures (*e.g.*, electrochemical interface in solid-state battery) in order to solve the nature of high-resolution interfaces. Third, integrated on-chip devices should become a reality at the applications end. The potential of an integrated device that is self-energized and can work independently (due to the incorporation of an energy harvesting unit, an energy storage unit, and a functional unit) is practically limitless—particularly if the micro/nano device is millimeter in size and micro/nano-watt in terms of power consumption. Consider the amazing implications, scientists should find ways to perfect their development and engineers seek to use them in implanted devices and micro-robots. Accordingly, the corresponding adjustment of device structure is necessary to adapt the demand of integration and monitoring. For application of on-chip micro-device, the stability and large-scale production of fabrication process should be set to the important subject of study. While the road is long to make that goal a reality, the potential of micro/nano devices is truly tantalizing.

Acknowledgements

This work was supported by the National Science Fund for Distinguished Young Scholars (51425204), the National Natural Science Foundation of China (51832004, 51802239), the National Key R&D Program of China (2016YFA0202603) and the Fundamental Research Funds for the Central Universities (WUT: 2019-zy-288). The authors would like to thank Prof. Bruce Dunn at University of California, Los Angeles, for his insightful discussion and support.

References

[1] N.S. Lewis, MRS Bull. 32 (2011) 808–820.
[2] D. Larcher, J.M. Tarascon, Nat. Chem. 7 (2015) 19–29.
[3] A. Midilli, I. Dincer, M. Ay, Energ. Policy 34 (2006) 3623–3633.
[4] J.P. Painuly, Renew. Energ. 24 (2001) 73–89.
[5] B. Dunn, H. Kamath, J.-M. Tarascon, Science 334 (2011) 928–935.
[6] A. Khaligh, Z. Li, IEEE T. Veh. Technol. 59 (2010) 2806–2814.
[7] G. Rothenberg, Catalysis: Concepts and Green Applications, Ed., John Wiley & Sons, 2017.
[8] P. Simon, Y. Gogotsi, B. Dunn, Science 343 (2014) 1210–1211.
[9] K. B, C. G, Nature 458 (2009) 190–193.
[10] L. Mai, M. Yan, Y. Zhao, Nature 546 (2017) 469.
[11] L. Mai, J. Sheng, L. Xu, S. Tan, J. Meng, Acc. Chem. Res. 51 (2018) 950.
[12] C.Y. Wang, G. Zhang, S. Ge, T. Xu, Y. Ji, X.G. Yang, Y. Leng, Nature 529 (2016) 515–518.
[13] N. Liu, Z. Lu, J. Zhao, M.T. McDowell, H.W. Lee, W. Zhao, Y. Cui, Nat. Nanotechnol. 9 (2014) 187–192.
[14] P. Simon, Y. Gogotsi, Nat. Mater. 7 (2008) 845–854.
[15] J.R. Miller, P. Simon, Science 321 (2008) 651–652.
[16] K. Xiang, Z. Xu, T. Qu, Z. Tian, Y. Zhang, Y. Wang, M. Xie, X. Guo, W. Ding, X. Guo, Chem. Commun. (Camb.) 53 (2017) 12410–12413.
[17] Y. Zhang, T. Qu, K. Xiang, Y. Shen, S. Chen, M. Xie, X. Guo, J. Mater. Chem. A Mater. Energy Sustain. 6 (2018) 2353–2359.
[18] L. Zhou, K. Zhang, Z. Hu, Z. Tao, L. Mai, Y.M. Kang, S.L. Chou, J. Chen,Adv. Energy Mater. 8 (2018), 1701415.
[19] M. Xie, Z. Xu, S. Duan, Z. Tian, Y. Zhang, K. Xiang, M. Lin, X. Guo, W. Ding, Nano Res. 11 (2018) 216–224.
[20] M. Xie, S. Duan, Y. Shen, K. Fang, Y. Wang, M. Lin, X. Guo, ACS Energy Lett. 1 (2016) 814–819.
[21] Y.K. Sun, Z. Chen, H.J. Noh, D.J. Lee, H.G. Jung, Y. Ren, S. Wang, C.S. Yoon, S.T. Myung, K. Amine, Nat. Mater. 11 (2012) 942–947.
[22] J.B. Goodenough, Y. Kim, Chem. Mater. 22 (2010) 587–603.
[23] Y. Sun, N. Liu, Y. Cui, Nat. Energy 1 (2016) 16071.
[24] A. Kwade, W. Haselrieder, R. Leithoff, A. Modlinger, F. Dietrich, K. Droeder, Nat. Energy 3 (2018) 290–300.
[25] H. Sun, J. Zhu, D. Baumann, L. Peng, Y. Xu, I. Shakir, Y. Huang, X. Duan, Nat. Rev. Mater. 4 (2019) 45–60.
[26] S.J.N.N. Bruno, Nat. Nanotechnol. 2 (2007) 598–599.
[27] L. Ma, K.E. Hendrickson, S. Wei, L.A. Archer, Nano Today 10 (2015) 315–338.
[28] Y. Gogotsi, R.M. Penner, ACS Nano 12 (2018) 2081–2083.
[29] N. Li, C.R. Martin, B. Scrosati, J. Power Sources 97–98 (2001) 240–243.
[30] C. Jiang, E. Hosono, H. Zhou, Nano Today 1 (2006) 28–33.
[31] G. Cao, Nanostructures and Nanomaterials: Synthesis, Properties And Applications, ed., Imperial College Press, Singapore, 2004.
[32] M. Pumera, Energy Environ. Sci. 4 (2011) 668–674.
[33] X. Cao, C. Tan, X. Zhang, W. Zhao, H. Zhang, Adv. Mater. 47 (2016) 6167–6196.
[34] I. Ryu, J.W. Choi, Y. Cui, W.D. Nix, J. Mech. Phys. Solids 59 (2011) 1717–1730.
[35] S.-Y. Lee, L. Wu, A.S. Poyraz, J. Huang, A.C. Marschilok, K.J. Takeuchi, E.S. Takeuchi, M. Kim, Y. Zhu, Adv. Mater. 29 (2017).
[36] S. Xu, Y. Qin, C. Xu, Y. Wei, R. Yang, Z.L. Wang, Nat. Nanotechnol. 5 (2010) 366.
[37] J.M. Tarascon, M. Armand, Nature 414 (2001) 359.
[38] N. Nitta, F. Wu, J.T. Lee, G. Yushin, Mater. Today 18 (2015) 252–264.
[39] H. Sun, L. Mei, J. Liang, Z. Zhao, C. Lee, H. Fei, M. Ding, J. Lau, M. Li, C. Wang, X. Xu, G. Hao, B. Papandrea, I. Shakir, B. Dunn, Y. Huang, X. Duan, Science 356 (2017) 599–604.
[40] Y. Xia, T.S. Mathis, M.-Q. Zhao, B. Anasori, A. Dang, Z. Zhou, H. Cho, Y. Gogotsi, S. Yang, Nature 557 (2018) 409–412.
[41] H. Li, Joule 3 (2019) 911–914.
[42] J. Wang, M.S. Gudiksen, X. Duan, Y. Cui, C.M. Lieber, Science 293 (2001) 1455–1457.
[43] L. Liao, Y.C. Lin, M. Bao, R. Cheng, J. Bai, Y. Liu, Y. Qu, K.L. Wang, Y. Huang, X. Duan, Nature 467 (2010) 305–308.
[44] Y. Liu, J. Guo, Q. He, H. Wu, H.C. Cheng, M. Ding, I. Shakir, V. Gambin, Y. Huang, X. Duan, Nano Lett. 17 (2017) 5495–5501.
[45] K.S. Novoselov, A.K. Geim, S.V. Morozov, D. Jiang, Y. Zhang, S.V. Dubonos, I.V. Grigorieva, A.A. Firsov, Science 306 (2004) 666–669.
[46] Y. Cao, V. Fatemi, A. Demir, S. Fang, S.L. Tomarken, J.Y. Luo, J.D. Sanchez-Yamagishi, K. Watanabe, T. Taniguchi, E. Kaxiras, R.C. Ashoori, P. Jarillo-Herrero, Nature 556 (2018) 80.
[47] B. Radisavljevic, A. Radenovic, J. Brivio, V. Giacometti, A. Kis, Nat. Nanotechnol. 6 (2011) 147–150.
[48] K. Liu, Y. Liu, D. Lin, A. Pei, Y. Cui, Sci. Adv. 4 (2018) eaas9820.
[49] M. Winter, B. Barnett, K. Xu, Chem. Rev. 118 (2018) 11433–11456.
[50] L. Mai, Y. Dong, L. Xu, C. Han, Nano Lett. 10 (2010) 4273–4278.
[51] A.D. Handoko, F. Wei, B.S. Jenndy, Z.W. Yeo, Seh, Nat. Catal. 1 (2018) 922–934.
[52] R. Bhattacharyya, B. Key, H. Chen, A.S. Best, A.F. Hollenkamp, C.P. Grey, Nat. Mater. 9 (2010) 504–510.
[53] J.Y. Huang, L. Zhong, C.M. Wang, J.P. Sullivan, W. Xu, L.Q. Zhang, S.X. Mao, N.S. Hudak, X.H. Liu, A. Subramanian, Science 330 (2010) 1515–1520.
[54] H. Ghassemi, M. Au, N. Chen, P.A. Heiden, R.S. Yassar, ACS Nano 5 (2011) 7805–7811.
[55] P. Parkinson, Y.-H. Lee, L. Fu, S. Breuer, H.H. Tan, C. Jagadish, Nano Lett. 13 (2013) 1405–1409.
[56] Y. Deng, A.D. Handoko, Y. Du, S. Xi, B.S. Yeo, ACS Catal. 6 (2016) 2473–2481.
[57] K. Amine, I. Belharouak, Z. Chen, T. Tran, H. Yumoto, N. Ota, S.-T. Myung, Y.-K. Sun, Adv. Mater. 22 (2010) 3052–3057.
[58] G. Segev, J.W. Beeman, J.B. Greenblatt, I.D. Sharp, Nat. Mater. 17 (2018) 1115–1121.
[59] S.D. Beattie, M.J. Loveridge, M.J. Lain, S. Ferrari, B.J. Polzin, R. Bhagat, R. Dashwood, J. Power Sources 302 (2016) 426–430.
[60] Y. Hoshi, Y. Narita, K. Honda, T. Ohtaki, I. Shitanda, M. Itagaki, J. Power Sources 288 (2015) 168–175.
[61] N.A. Kyerematen, T. Brousse, D. Pech, Nat. Nanotechnol. 12 (2016) 7.
[62] P. Wang, M. Yan, J. Meng, G. Jiang, L. Qu, X. Pan, J.Z. Liu, L. Mai, Nat. Commun. 8 (2017) 645.
[63] P. Krogstrup, H.I. Jørgensen, M. Heiss, O. Demichel, J.V. Holm, M. Aagesen, J. Nygard, A. Fontcuberta i Morral, Nat. Photonics 7 (2013) 306–310.
[64] Y. Su, C. Liu, S. Brittman, J. Tang, A. Fu, N. Kornienko, Q. Kong, P. Yang, Nat. Nanotechnol. 11 (2016) 609–612.
[65] K.S. Novoselov, A. Mishchenko, A. Carvalho, A.H. Castro Neto, Science 353 (2016) aac9439.
[66] Y. Liu, N.O. Weiss, X. Duan, H.-C. Cheng, Y. Huang, X. Duan, Nat. Rev. Mater. 1 (2016) 16042.
[67] P.J. Zomer, M.H.D. Guimarães, J.C. Brant, N. Tombros, B.J.V. Wees, Appl. Phys. Lett. 105 (2014) 419.
[68] Y. Chen, Microelectron. Eng. 135 (2015) 57–72.
[69] C. Vieu, F. Carcenac, A. Pépin, Y. Chen, M. Mejias, A. Lebib, L. Manin-Ferlazzo, L. Couraud, H. Launois, Appl. Surf. Sci. 164 (2000) 111–117.
[70] C.D. English, G. Shine, V.E. Dorgan, K.C. Saraswat, E. Pop, Nano Lett. 16 (2016) 3824–3830.
[71] M.B.E. Griffiths, P.J. Pallister, D.J. Mandia, S.T. Barry, Chem. Mater. 28 (2016) 44–46.
[72] X. Tian, M. Shi, X. Xu, M. Yan, L. Xu, A. Minhas-Khan, C. Han, L. He, L. Mai, Adv. Mater. 27 (2015) 7476–7482.
[73] A.S. Aricò, P. Bruce, B. Scrosati, J.M. Tarascon, S.W. Van, Nat. Mater. 4 (2005) 366–377.
[74] W. Li, J. Liu, D. Zhao, Nat. Rev. Mater. 1 (2016) 16023.
[75] N.S. Lewis, Science 351 (2016).
[76] N.S. Lewis, D.G. Nocera, P. Natl, Acad. Sci. USA 103 (2006) 15729–15735.
[77] M.A. Green, Y. Hishikawa, W. Warta, E.D. Dunlop, D.H. Levi, J. Hohl-Ebinger, A.W. Ho-Baillie, Prog. Photovolt. Res. Appl. 25 (2017) 668–676.
[78] K. Yoshikawa, H. Kawasaki, W. Yoshida, T. Irie, K. Konishi, K. Nakano, T. Uto, D. Adachi, M. Kanematsu, H. Uzu, Nat. Energy 2 (2017) 17032.
[79] M.A. Green, S.P. Bremner, Nat. Mater. 16 (2017) 23.
[80] G. Conibeer, M. Green, R. Corkish, Y. Cho, E.-C. Cho, C.-W. Jiang, T. Fangsuwannarak, E. Pink, Y. Huang, T. Puzzer, Thin Solid Films 511 (2006) 654–662.
[81] B. Tian, T.J. Kempa, C.M. Lieber, Chem. Soc. Rev. 38 (2009) 16–24.
[82] L. Hu, G. Chen, Nano Lett. 7 (2007) 3249–3252.

Please cite this article in press as: X. Pan, et al., On-chip micro/nano devices for energy conversion and storage, Nano Today (xxxx), https://doi.org/10.1016/j.nantod.2019.100764

[83] B. Tian, X. Zheng, T.J. Kempa, Y. Fang, N. Yu, G. Yu, J. Huang, C.M. Lieber, Nature 449 (2007) 885–889.
[84] A. Polman, H.A. Atwater, Nat. Mater. 11 (2012) 174.
[85] Z. Zhong, Z. Li, Q. Gao, Z. Li, K. Peng, L. Li, S. Mokkapati, K. Vora, J. Wu, G. Zhang, Z. Wang, L. Fu, H.H. Tan, C. Jagadish, Nano Energy 28 (2016) 106–114.
[86] S.A. Mann, S.Z. Oener, A. Cavalli, J.E. Haverkort, E.P. Bakkers, E.C. Garnett, Nat. Nanotechnol. 11 (2016) 1071–1075.
[87] I. Thomann, B.A. Pinaud, Z. Chen, B.M. Clemens, T.F. Jaramillo, M.L. Brongersma, Nano Lett. 11 (2011) 3440–3446.
[88] M. Ni, M.K.H. Leung, D.Y.C. Leung, K. Sumathy, Renew. Sust. Energ. Rev. 11 (2007) 401–425.
[89] Y.X. Pan, Y. You, S. Xin, Y. Li, G. Fu, Z. Cui, Y.L. Men, F.F. Cao, S.H. Yu, J.B. Goodenough, J. Am. Chem. Soc. 139 (2017) 4123–4129.
[90] J. Tian, Q. Liu, A.M. Asiri, X. Sun, J. Am. Chem. Soc. 136 (2014) 7587–7590.
[91] M. Kibria, F. Chowdhury, S. Zhao, B. AlOtaibi, M. Trudeau, H. Guo, Z. Mi, Nat. Commun. 6 (2015) 6797.
[92] Q. Hu, H. Wu, J. Sun, D. Yan, Y. Gao, J. Yang, Nanoscale 8 (2016) 5350–5357.
[93] A.K. Singh, K. Mathew, H.L. Zhuang, R.G. Hennig, J. Phys. Chem. L 6 (2015) 1087–1098.
[94] L. Qipeng, Y. Yifu, M. Qinglang, C. Bo, Z. Hua, Adv. Mater. 28 (2016) 1917–1933.
[95] A.T. Valota, P.S. Toth, Y.-J. Kim, B.H. Hong, I.A. Kinloch, K.S. Novoselov, E.W. Hill, R.A.W. Dryfe, Electrochim. Acta 110 (2013) 9–15.
[96] M. Velický, D.F. Bradley, A.J. Cooper, E.W. Hill, I.A. Kinloch, A. Mishchenko, K.S. Novoselov, H.V. Patten, P.S. Toth, A.T. Valota, S.D. Worrall, R.A.W. Dryfe, ACS Nano 8 (2014) 10089–10100.
[97] P.S. Toth, A.T. Valota, M. Velický, I.A. Kinloch, K.S. Novoselov, E.W. Hill, R.A.W. Dryfe, Chem. Sci. 5 (2014) 582–589.
[98] M. Velický, A.J. Cooper, P.S. Toth, H.V. Patten, C.R. Woods, K.S. Novoselov, R.A.W. Dryfe,2d Mater. 2 (2015), 024011.
[99] M. Velicky, M.A. Bissett, P.S. Toth, H.V. Patten, S.D. Worrall, A.N. Rodgers, E.W. Hill, I.A. Kinloch, K.S. Novoselov, T. Georgiou, L. Britnell, R.A. Dryfe, Phys. Chem. Chem. Phys. 17 (2015) 17844–17853.
[100] M. Velicky, M.A. Bissett, C.R. Woods, P.S. Toth, T. Georgiou, I.A. Kinloch, K.S. Novoselov, R.A. Dryfe, Nano Lett. 16 (2016) 2023–2032.
[101] R.E.H. Sims, H.-H. Rogner, K. Gregory, Energ. Policy 31 (2003) 1315–1326.
[102] B. Poudel, Q. Hao, Y. Ma, Y. Lan, A. Minnich, B. Yu, X. Yan, D. Wang, A. Muto, D. Vashaee, Science 320 (2008) 634–638.
[103] G.J. Snyder, E.S. Toberer, Nat. Mater. 7 (2008) 105.
[104] K.F. Hsu, S. Loo, F. Guo, W. Chen, J.S. Dyck, C. Uher, T. Hogan, E. Polychroniadis, M.G. Kanatzidis, Science 303 (2004) 818–821.
[105] R. Chen, J. Lee, W. Lee, D. Li, Chem. Rev. (2019).
[106] A.I. Hochbaum, R. Chen, R.D. Delgado, W. Liang, E.C. Garnett, M. Najarian, A. Majumdar, P. Yang, Nature 451 (2008) 163–167.
[107] L. Liu, K.Q. Peng, Y. Hu, X.L. Wu, S.T. Lee, Adv. Mater. 26 (2014) 1410–1413.
[108] A. Sood, J. Cho, K.D. Hobart, T.I. Feygelson, B.B. Pate, M. Asheghi, D.G. Cahill, K.E. Goodson,J. Appl. Phys. 119 (2016), 175103.
[109] V. Meunier, A. Souza Filho, E. Barros, M. Dresselhaus,Rev. Mod. Phys. 88 (2016), 025005.
[110] K.F. Mak, C. Lee, J. Hone, J. Shan, T.F. Heinz,Phys. Rev. Lett. 105 (2010), 136805.
[111] J.K. Ellis, M.J. Lucero, G.E. Scuseria,Appl. Phys. Lett. 99 (2011), 261908.
[112] C. Lee, H. Yan, L.E. Brus, T.F. Heinz, J. Hone, S. Ryu, ACS Nano 4 (2010) 2695–2700.
[113] S. Shimizu, T. Iizuka, K. Kanahashi, J. Pu, K. Yanagi, T. Takenobu, Y. Iwasa, Small 12 (2016) 3388–3392.
[114] A. Askounis, Y. Yamada, T. Ikuta, K. Takahashi, Y. Takata, K. Sefiane,AIP Adv. 6 (2016), 115119.
[115] W. Park, D.D. Shin, S.J. Kim, J.S. Katz, J. Park, C.H. Ahn, T. Kodama, M. Asheghi, T.W. Kenny, K.E. Goodson,Appl. Phys. Lett. 110 (2017), 213102.
[116] X. Xu, L.F. Pereira, Y. Wang, J. Wu, K. Zhang, X. Zhao, S. Bae, C.T. Bui, R. Xie, J.T. Thong, Nat. Commun. 5 (2014) 3689.
[117] S. Ghosh, W. Bao, D.L. Nika, S. Subrina, E.P. Pokatilov, C.N. Lau, A.A. Balandin, Nat. Mater. 9 (2010) 555–558.
[118] L. Hicks, M.S. Dresselhaus, J. Phys. Chem. B 47 (1993) 12727.
[119] J. Sofo, G. Mahan, Appl. Phys. Lett. 65 (1994) 2690–2692.
[120] J. Zeng, X. He, S.-J. Liang, E. Liu, Y. Sun, C. Pan, Y. Wang, T. Cao, X. Liu, C. Wang, Nano Lett. 18 (2018) 7538–7545.
[121] M. Sadrzadeh, T. Mohammadi, Desalination 221 (2008) 440–447.
[122] C. Charcosset, Desalination 245 (2009) 214–231.
[123] Z. Jia, B. Wang, S. Song, Y. Fan, Renew. Sust. Energ. Rev. 31 (2014) 91–100.
[124] J.W. Post, Blue Energy: Electricity Production From Salinity Gradients by Reverse Electrodialysis, Ed., 2009.
[125] M. Heiranian, A.B. Farimani, N.R. Aluru, Nat. Commun. 6 (2015) 8616.
[126] A. Aliprandi, D. Pakulski, A. Ciesielski, P. Samori, ACS Nano 11 (2017) 10654–10658.
[127] J. Feng, M. Graf, K. Liu, D. Ovchinnikov, D. Dumcenco, M. Heiranian, V. Nandigana, N.R. Aluru, A. Kis, A. Radenovic, Nature 536 (2016) 197–200.
[128] K.A. Mahmoud, B. Mansoor, A. Mansour, M. Khraisheh, Desalination 356 (2015) 208–225.
[129] A.S. Kazemi, Y. Abdi, J. Eslami, R. Das, Desalination (2018).
[130] D. Cohen-Tanugi, J.C. Grossman, Nano Lett. 12 (2012) 3602–3608.
[131] J.S. Bunch, S.S. Verbridge, J.S. Alden, A.M. Van Der Zande, J.M. Parpia, H.G. Craighead, P.L. McEuen, Nano Lett. 8 (2008) 2458–2462.
[132] S. Hu, M. Lozada-Hidalgo, F.C. Wang, A. Mishchenko, F. Schedin, R.R. Nair, E.W. Hill, D.W. Boukhvalov, M.I. Katsnelson, R.A. Dryfe, I.V. Grigorieva, H.A. Wu, A.K. Geim, Nature 516 (2014) 227–230.
[133] Y. Jiao, Y. Zheng, M. Jaroniec, S.Z. Qiao, Chem. Soc. Rev. 44 (2015) 2060–2086.
[134] X. Zou, Y. Zhang, Chem. Soc. Rev. 44 (2015) 5148–5180.
[135] T. Bak, J. Nowotny, M. Rekas, C. Sorrell, Int. J. Hydrogen Energ. 27 (2002) 991–1022.
[136] S.U. Khan, M. Al-Shahry, W.B. Ingler, Science 297 (2002) 2243–2245.
[137] A.J. Bard, M.A. Fox, Acc. Chem. Res. 28 (1995) 141–145.
[138] J. Greeley, T.F. Jaramillo, J. Bonde, I.B. Chorkendorff, J.K. Norskov, Nat. Mater. 5 (2006) 909–913.
[139] W.T. Hong, M. Risch, K.A. Stoerzinger, A. Grimaud, S. Jin, S.H. Yang, Energy Environ. Sci. 8 (2015) 1404–1427.
[140] K.A. Stoerzinger, M. Risch, B. Han, Y. Shao-Horn, ACS Catal. 5 (2015) 6021–6031.
[141] D.V. Esposito, S.T. Hunt, A.L. Stottlemyer, K.D. Dobson, B.E. McCandless, R.W. Birkmire, J.G. Chen, Angew. Chemie Int. Ed. English 49 (2010) 9859–9862.
[142] H. Yin, S. Zhao, K. Zhao, A. Muqsit, H. Tang, L. Chang, H. Zhao, Y. Gao, Z. Tang, Nat. Commun. 6 (2015) 6430.
[143] W.F. Chen, K. Sasaki, C. Ma, A.I. Frenkel, N. Marinkovic, J.T. Muckerman, Y. Zhu, R.R. Adzic, Angew. Chemie Int. Ed. English 51 (2012) 6131–6135.
[144] Y. Huang, R.J. Nielsen, W.A.I. Goddard, M.P. Soriaga, J. Am. Chem. Soc. 137 (2015) 6692–6698.
[145] Z. Chen, D. Cummins, B.N. Reinecke, E. Clark, M.K. Sunkara, T.F. Jaramillo, Nano Lett. 11 (2011) 4168–4175.
[146] T.F. Jaramillo, K.P. Jorgensen, J. Bonde, J.H. Nielsen, S. Horch, I. Chorkendorff, Science 317 (2007) 100–102.
[147] J. Zhang, J. Wu, H. Guo, W. Chen, J. Yuan, U. Martinez, G. Gupta, A. Mohite, P.M. Ajayan, J. Lou,Adv. Mater. 29 (2017), 1701955.
[148] D. Voiry, M. Salehi, R. Silva, T. Fujita, M. Chen, T. Asefa, V.B. Shenoy, G. Eda, M. Chhowalla, Nano Lett. 13 (2013) 6222–6227.
[149] D. Voiry, H. Yamaguchi, J. Li, R. Silva, D.C. Alves, T. Fujita, M. Chen, T. Asefa, V.B. Shenoy, G. Eda, Nat. Mater. 12 (2013) 850.
[150] C. Tsai, K. Chan, J.K. Nørskov, F. Abild-Pedersen, Surf. Sci. 640 (2015) 133–140.
[151] D. Voiry, R. Fullon, J. Yang, E.S.C. de Carvalho Castro, R. Kappera, I. Bozkurt, D. Kaplan, M.J. Lagos, P.E. Batson, G. Gupta, A.D. Mohite, L. Dong, D. Er, V.B. Shenoy, T. Asefa, M. Chhowalla, Nat. Mater. 15 (2016) 1003–1009.
[152] Y. Yu, G.-H. Nam, Q. He, X.-J. Wu, K. Zhang, Z. Yang, J. Chen, Q. Ma, M. Zhao, Z. Liu, Nat. Chem. 10 (2018) 638.
[153] Y. Katagiri, T. Nakamura, A. Ishii, C. Ohata, M. Hasegawa, S. Katsumoto, T. Cusati, A. Fortunelli, G. Iannaccone, G. Fiori, S. Roche, J. Haruyama, Nano Lett. 16 (2016) 3788–3794.
[154] Y.J. Zhang, J.T. Ye, Y. Yomogida, T. Takenobu, Y. Iwasa, Nano Lett. 13 (2013) 3023–3028.
[155] A. Dankert, S.P. Dash, Nat. Commun. 8 (2017) 16093.
[156] Z. Yu, Z.Y. Ong, S. Li, J.B. Xu, G. Zhang, Y.W. Zhang, Y. Shi, X. Wang, Adv. Funct. Mater. 27 (2017).
[157] L. Britnell, R.V. Gorbachev, R. Jalil, B.D. Belle, F. Schedin, A. Mishchenko, T. Georgiou, M.I. Katsnelson, L. Eaves, S.V. Morozov, Science 335 (2012) 947–950.
[158] J. Jeong, N. Aetukuri, T. Graf, T.D. Schladt, M.G. Samant, S.S. Parkin, Science 339 (2013) 1402–1405.
[159] D.R. Cummins, U. Martinez, A. Sherehiy, R. Kappera, A. Martinez-Garcia, R.K. Schulze, J. Jasinski, J. Zhang, R.K. Gupta, J. Lou, Nat. Commun. 7 (2016) 11857.
[160] J. Wang, M. Yan, K. Zhao, X. Liao, P. Wang, X. Pan, W. Yang, L. Mai,Adv. Mater. 29 (2017), 1604464.
[161] M. Yan, X. Pan, P. Wang, F. Chen, L. He, G. Jiang, J. Wang, J.Z. Liu, X. Xu, X. Liao, Nano Lett. 17 (2017) 4109–4115.
[162] M. Yan, X. Zhou, X. Pan, J. Wang, L. Xia, K. Yu, X. Liao, X. Xu, L. He, L. Mai, Nano Res. (2017).
[163] Y. He, Q. He, L. Wang, C. Zhu, P. Golani, A.D. Handoko, X. Yu, C. Gao, M. Ding, X. Wang, F. Liu, Q. Zeng, P. Yu, S. Guo, B.I. Yakobson, L. Wang, Z.W. Seh, Z. Zhang, M. Wu, Q.J. Wang, H. Zhang, Z. Liu, Nat. Mater (2019), http://dx.doi.org/10.1038/s41563-019-0426-0.
[164] Y. Zhou, J.L. Silva, J.M. Woods, J.V. Pondick, Q. Feng, Z. Liang, W. Liu, L. Lin, B. Deng, B. Brena,Adv. Mater. (2018), 1706076.
[165] M. Ding, Q. He, G. Wang, H.C. Cheng, Y. Huang, X. Duan, Nat. Commun. 6 (2015) 1–9.
[166] M. Ding, G. Zhong, Z. Zhao, Z. Huang, M. Li, H.-Y. Shiu, Y. Liu, I. Shakir, Y. Huang, X. Duan, ACS Central Sci. 4 (2018) 590–599.
[167] R. Zhang, Q. Wen, W. Qian, D.S. Su, Q. Zhang, F. Wei, Adv. Mater. 23 (2011) 3387–3391.
[168] L.Q. Mai, F. Yang, Y.L. Zhao, X. Xu, L. Xu, Y.Z. Luo, Nat. Commun. 2 (2011) 381.
[169] K. Pielichowska, K. Pielichowski, Prog. Mater. Sci. 65 (2014) 67–123.
[170] Z. Liu, Y. Zhan, G. Shi, S. Moldovan, M. Gharbi, L. Song, L. Ma, W. Gao, J. Huang, R. Vajtai, F. Banhart, P. Sharma, J. Lou, P.M. Ajayan, Nat. Commun. 3 (2012) 879.
[171] Y. Idota, Science 276 (1997) 1395–1397.
[172] H. Wang, Q. Gao, L. Jiang, Small 7 (2011) 2454–2459.
[173] C.K. Chan, H. Peng, G. Liu, K. McIlwrath, X.F. Zhang, R.A. Huggins, Y. Cui, Nat. Nanotechnol. 3 (2008) 31.
[174] Y. Xia, Y. Zhou, M. Yoshio, J. Electrochem. Soc. 144 (1997) 2593–2600.
[175] Y. Zhao, C. Han, J. Yang, J. Su, X. Xu, S. Li, L. Xu, R. Fang, H. Jiang, X. Zou, Nano Lett. 15 (2015) 2180–2185.
[176] X. Xu, M. Yan, X. Tian, C. Yang, M. Shi, Q. Wei, X. Lin, L. Mai, Nano Lett. 15 (2015) 3879.
[177] Y. Hou, R. Xiao, X. Tong, S. Dhuey, D. Yu, Nano Lett. 17 (2017) 7702–7709.

Please cite this article in press as: X. Pan, et al., On-chip micro/nano devices for energy conversion and storage, Nano Today (xxxx), https://doi.org/10.1016/j.nantod.2019.100764

[178] P. Hu, T. Zhu, X. Wang, X. Wei, M. Yan, J. Li, W. Luo, W. Yang, W. Zhang, L. Zhou, Nano Lett. 18 (2018) 1758–1763.
[179] P. Hu, M. Yan, X. Wang, C. Han, L. He, X. Wei, C. Niu, K. Zhao, X. Tian, Q. Wei, Z. Li, L. Mai, Nano Lett. 16 (2016) 1523–1529.
[180] M. Yan, F. Wang, C. Han, X. Ma, X. Xu, Q. An, L. Xu, C. Niu, Y. Zhao, X. Tian, P. Hu, H. Wu, L. Mai, J. Am. Chem. Soc. 135 (2013) 18176–18182.
[181] X.B. Liao, Y.L. Zhao, J.H. Wang, W. Yang, L. Xu, X.C. Tian, Y. Shuang, K.A. Owusu, M.Y. Yan, L.Q. Mai, Nano Res. 11 (2018) 2083–2092.
[182] J. Wan, W. Bao, Y. Liu, J. Dai, F. Shen, L. Zhou, X. Cai, D. Urban, Y. Li, K. Jungjohann, M.S. Fuhrer, L. Hu,Adv. Energy Mater. 5 (2015), 1401742.
[183] M. Kuhne, F. Paolucci, J. Popovic, P.M. Ostrovsky, J. Maier, J.H. Smet, Nat. Nanotechnol. 12 (2017) 895–900.
[184] L. Wang, Z. Xu, W. Wang, X. Bai, J. Am. Chem. Soc. 136 (2014) 6693–6697.
[185] D. Sun, D.L. Ye, P. Liu, Y.G. Tang, J. Guo, L.Z. Wang, H.Y. Wang, Adv. Energy Mater. 8 (2018).
[186] Y.C. Lin, D.O. Dumcenco, Y.S. Huang, K. Suenaga, Nat. Nanotechnol. 9 (2014) 391–396.
[187] W. Bao, J. Wan, X. Han, X. Cai, H. Zhu, D. Kim, D. Ma, Y. Xu, J.N. Munday, H.D. Drew, M.S. Fuhrer, L. Hu, Nat. Commun. 5 (2014) 4224.
[188] F. Xiong, H. Wang, X. Liu, J. Sun, M. Brongersma, E. Pop, Y. Cui, Nano Lett. 15 (2015) 6777–6784.
[189] M. Kühne, F. Börrnert, S. Fecher, M. Ghorbani-Asl, J. Biskupek, D. Samuelis, A.V. Krasheninnikov, U. Kaiser, J.H. Smet, Nature 564 (2018) 234–239.
[190] N.A. Kyeremateng, T. Brousse, D. Pech, Nat. Nanotechnol. 12 (2017) 7–15.
[191] Q. Meng, H. Wu, Y. Meng, K. Xie, Z. Wei, Z. Guo, Adv. Mater. 26 (2014) 4100–4106.
[192] K. Shen, J. Ding, S. Yang,Adv. Energy Mater. (2018), 1800408.
[193] D.P. Dubal, O. Ayyad, V. Ruiz, P. Gomez-Romero, Chem. Soc. Rev. 44 (2015) 1777–1790.
[194] H. Pan, D. Wang, Q. Peng, J. Ma, X. Meng, Y. Zhang, Y. Ma, S. Zhu, D. Zhang, ACS Appl. Mater. Inter. 10 (2018) 10157–10164.
[195] H. Xiao, Z.S. Wu, L. Chen, F. Zhou, S. Zheng, W. Ren, H.M. Cheng, X. Bao, ACS Nano 11 (2017) 7284–7292.
[196] Y. Lin, Y. Gao, Z. Fan,Adv. Mater. 29 (2017), 1701736.
[197] S. Wang, Z.-S. Wu, F. Zhou, X. Shi, S. Zheng, J. Qin, H. Xiao, C. Sun, X. Bao, npj 2D Mater. Appl. 2 (2018) 7.
[198] S. Zheng, J. Ma, Z.-S. Wu, F. Zhou, Y.-B. He, F. Kang, H.-M. Cheng, X. Bao, Energy Environ. Sci. (2018), http://dx.doi.org/10.1039/c1038ee00855h.
[199] Y. Wei, H. Liang, X. Tian, M. Yan, Y. Hui, X. Liao, J. Meng, Z. Hao, L. Mai, Small 13 (2017).
[200] Y. Yang, L. He, C. Tang, P. Hu, X. Hong, M. Yan, Y. Dong, X. Tian, Q. Wei, L. Mai, Nano Res. 9 (2016) 2510–2519.
[201] X. Hong, L. He, X. Ma, W. Yang, Y. Chen, L. Zhang, H. Yan, Z. Li, L. Mai, Nano Res. 10 (2017) 3743–3753.
[202] J. Zhu, Z.C. Wang, H. Dai, Q. Wang, R. Yang, H. Yu, M. Liao, J. Zhang, W. Chen, Z. Wei, N. Li, L. Du, D. Shi, W. Wang, L. Zhang, Y. Jiang, G. Zhang, Nat. Commun. 10 (2019) 1348.
[203] G.-H. Nam, Q. He, X. Wang, Y. Yu, J. Chen, K. Zhang, Z. Yang, D. Hu, Z. Lai, B. Li, Q. Xiong, Q. Zhang, L. Gu, H. Zhang,Adv. Mater. 0 (2019), 1807764.
[204] D. Hu, T. Zhao, X. Ping, H. Zheng, L. Xing, X. Liu, J. Zheng, L. Sun, L. Gu, C. Tao, D. Wang, L. Jiao, Small (2019).
[205] Y. Zhou, J.V. Pondick, J.L. Silva, J.M. Woods, D.J. Hynek, G. Matthews, X. Shen, Q. Feng, W. Liu, Z. Lu, Z. Liang, B. Brena, Z. Cai, M. Wu, L. Jiao, S. Hu, H. Wang, C.M. Araujo, J.J. Cha,Small 0 (2019), 1900078.
[206] M. Ding, G. Zhong, Z. Zhao, Z. Huang, M. Li, H.Y. Shiu, Y. Liu, I. Shakir, Y. Huang, X. Duan, ACS Cent. Sci. 4 (2018) 590–599.
[207] K. Shen, J. Ding, S. Yang,Adv. Energy Mater. 8 (2018), 1800408.
[208] D. Zhao, C. Chen, Q. Zhang, W. Chen, S. Liu, Q. Wang, Y. Liu, J. Li, H. Yu,Adv. Energy Mater. 7 (2017), 1700739.
[209] C.J. Zhang, M.P. Kremer, A. Seral-Ascaso, S.-H. Park, N. McEvoy, B. Anasori, Y. Gogotsi, V. Nicolosi,Adv. Funct. Mater. 28 (2018), 1705506.
[210] Y. Lin, Y. Gao, Z. Fan, Adv. Mater. 29 (2017).
[211] J. Yoo, S. Byun, C.-W. Lee, C.-Y. Yoo, J. Yu, Chem. Mater. 30 (2018) 3979–3990.
[212] Y. Yue, N. Liu, Y. Ma, S. Wang, W. Liu, C. Luo, H. Zhang, F. Cheng, J. Rao, X. Hu, J. Su, Y. Gao, ACS Nano 12 (2018) 4224–4232.
[213] R. Guo, J. Chen, B. Yang, L. Liu, L. Su, B. Shen, X. Yan,Adv. Funct. Mater. 27 (2017), 1702394.
[214] T. Purkait, G. Singh, N. Kamboj, M. Das, R.S. Dey, J. Mater. Chem. A 6 (2018) 22858–22869.
[215] J. Gao, C. Shao, S. Shao, F. Wan, C. Gao, Y. Zhao, L. Jiang, L. Qu,Small 14 (2018), e1801809.
[216] S. Wang, Z.-S. Wu, F. Zhou, X. Shi, S. Zheng, J. Qin, H. Xiao, C. Sun, X. Bao, npj 2D Mater. Appl. 2 (2018).
[217] F. Zhou, H. Huang, C. Xiao, S. Zheng, X. Shi, J. Qin, Q. Fu, X. Bao, X. Feng, K. Mullen, Z.S. Wu, J. Am. Chem. Soc. 140 (2018) 8198–8205.
[218] M. Zhu, Y. Huang, Y. Huang, H. Li, Z. Wang, Z. Pei, Q. Xue, H. Geng, C. Zhi, Adv. Mater. 29 (2017).
[219] R.K. Pal, S.C. Kundu, V.K. Yadavalli, ACS Appl. Mater. Inter. 10 (2018) 9620–9628.
[220] P. Zhang, J. Wang, W. Sheng, F. Wang, J. Zhang, F. Zhu, X. Zhuang, R. Jordan, O.G. Schmidt, X. Feng, Energy Environ. Sci. 11 (2018) 1717–1722.
[221] J. Li, S. Sollami Delekta, P. Zhang, S. Yang, M.R. Lohe, X. Zhuang, X. Feng, M. Ostling, ACS Nano 11 (2017) 8249–8256.
[222] Y. Wang, Y.-Z. Zhang, D. Dubbink, J.E. ten Elshof, Nano Energy 49 (2018) 481–488.
[223] Y. Song, H. Chen, X. Chen, H. Wu, H. Guo, X. Cheng, B. Meng, H. Zhang, Nano Energy 53 (2018) 189–197.
[224] J. Ye, H. Tan, S. Wu, K. Ni, F. Pan, J. Liu, Z. Tao, Y. Qu, H. Ji, P. Simon, Y. Zhu,Adv. Mater. 30 (2018), e1801384.
[225] S. Lochmann, J. Grothe, K. Eckhardt, D. Leistenschneider, L. Borchardt, S. Kaskel, Nanoscale 10 (2018) 10109–10115.

Xuelei Pan obtained his Bachelor's degree from the International School of Materials Science and Engineering, Wuhan University of Technology in 2018. He is now a doctoral student at Wuhan University of Technology under the supervision of Prof. Liqiang Mai. His research interests focus on nanomaterials for electrocatalysis and on-chip nanodevices for electrochemistry.

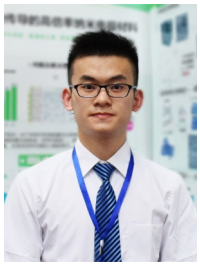

Xufeng Hong received his Bachelor's degree in Department of Materials Science and Engineering from Wuhan University of Technology (WUT) in 2018. He is currently working toward the Master degree. His current focus is micro energy storage devices such as micro-supercapacitors and micro-batteries.

Lin Xu received his Ph.D. degree in 2013 from School of Materials Science and Engineering at Wuhan University of Technology under the supervision of Professor Liqiang Mai, Professor Qingjie Zhang and Professor Charles M. Lieber. He was a visiting graduate student (2011–2013) and postdoctoral research fellow (2013–2016) in Lieber Research Group at Harvard University. He is currently a professor at State Key Laboratory of Advanced Technology for Materials Synthesis and Processing, Wuhan University of Technology. His research focuses on nanomaterials and devices for energy storage and conversion.

Yanxi Li received his Ph.D. degree in Materials Science and Engineering from Virginia Tech, USA in 2016. He is currently a postdoctoral research fellow at Department of Materials Science & Engineering and Geballe Laboratory for Advanced Materials (GLAM), Stanford University, USA. His current research interests focus on advanced materials for energy storage and epitaxial growth for functional thin films.

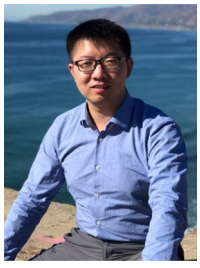

Mengyu Yan earned his Ph.D. degree from Wuhan University of Technology in 2017. He then carried out postdoctoral research in Prof. Jihui Yang's group at University of Washington. Currently, he is a WRF innovation fellow of clean energy institute at University of Washington. His research interests include the sub-nanoscale ion/charge transport in energy and biosystem.

Liqiang Mai is Chair Professor of Materials Science and Engineering at Wuhan University of Technology (WUT). He is the winner of the National Natural Science Fund for Distinguished Young Scholars and Fellow of the Royal Society of Chemistry. He received his Ph.D. from WUT in 2004 and carried out his postdoctoral research with Prof. Zhong Lin Wang at Georgia Institute of Technology in 2006–2007. He worked as an advanced research scholar with Prof. Charles M. Lieber at Harvard University in 2008–2011 and Prof. Peidong Yang at University of California, Berkeley in 2017. His current research interests focus on new nanomaterials for electrochemical energy storage and micro/nano energy devices.

Please cite this article in press as: X. Pan, et al., On-chip micro/nano devices for energy conversion and storage, Nano Today (xxxx), https://doi.org/10.1016/j.nantod.2019.100764